

Imbalanced Superfluid Phase of a Trapped Fermi Gas in the BCS-BEC Crossover Regime

Takeshi MIZUSHIMA*, Masanori ICHIOKA, and Kazushige MACHIDA

Department of Physics, Okayama University, Okayama 700-8530, Japan

(Received October 27, 2018)

We theoretically investigate the ground state of trapped neutral fermions with population imbalance in the BCS-BEC crossover regime. Based on the single-channel Hamiltonian, we perform fully numerical calculations of the Bogoliubov-de Gennes equation coupled with the regularized gap and number equations. The zero temperature phase diagram in the crossover regime is presented, where the Fulde-Ferrell-Larkin-Ovchinnikov (FFLO) pairing state governs the weak coupling BCS region of a resonance. It is found that the FFLO oscillation vanishes in the BEC side, in which the system under population imbalance turns into the phase separation (PS) between locally binding superfluid and fully polarized spin domains. We also demonstrate the numerical calculations with a large particle number $O(10^5)$ comparable with the recent experiments. The resulting density profile on a resonance yields the PS which is in good agreement with the recent experiments, while there exists the FFLO modulation in the pairing field. It is also proposed that the most favorable situation for the detection of the FFLO oscillation is in the vicinity of the critical population imbalance in the weak coupling BCS regime, where the oscillation periodicity becomes much larger than the interparticle spacing. Finally, we analyze the radio-frequency (RF) spectroscopy in the imbalanced system. The clear difference of the RF spectroscopy between BCS and BEC sides reveals the structure on the pairing field and local “magnetization”.

KEYWORDS: Quantum atomic gas, FFLO state, BCS-BEC crossover, imbalanced superfluid, Bogoliubov-de Gennes equation, phase diagram, radio-frequency spectroscopy

1. Introduction

There is increasing interest in the investigation of neutral Fermi systems with mismatched Fermi surfaces.¹ The robustness of superfluidity against the “paramagnetic” depairing is a longstanding fundamental issue, which has captured the attention of researchers in various fields, ranging from the condensed matter to the color superconductivity in dense quark matters.² Recently, superfluid phases under population imbalance has been realized in a trapped Fermi gas,^{3–8} accompanied with the manipulation of the s -wave scattering length a , by the Feshbach resonance.

For the achievement of superfluidity in neutral atom systems, the Feshbach resonance is a key factor. By applying the external magnetic field, this enables one to control the relative energy between two channels of the scattering process: The open (scattering) and closed (bound) channels. Two fermions distributed in hyperfine spin states labeled as $\sigma = \uparrow, \downarrow$ form the Cooper pair via the weak attractive interaction in the system with the negative a . In contrast, in the positive a , the energy of the closed channel, i.e., the binding energy, is characterized as $E_b = -1/Ma^2$ with the mass M , which leads to the stable formation of tightly bound molecular bosons. The composite bosons with long lifetime turns into the Bose-Einstein condensed phase below the critical temperature. Hence, the manipulation of interatomic interaction continuously changes the superfluidity from the fermionic Bardeen-Cooper-Schrieffer (BCS) type to molecular Bose-Einstein condensation (BEC)

through the unitary limit on resonance, i.e., the BCS-BEC crossover.⁹

In the actual experiment with the neutral atoms, the total particle number N is conserved. Applying the radio-frequency field, one can control the population difference between two hyperfine spin states, called the population imbalance,

$$P \equiv \frac{N_{\uparrow} - N_{\downarrow}}{N_{\uparrow} + N_{\downarrow}}, \quad (1)$$

where N_{σ} is the number for spin σ species. The negligible contribution of the dipole-dipole interaction leads to the conservation of population imbalance P throughout the typical experimental time scale. It is known that in the presence of population imbalance, i.e., $P \neq 0$, the uniform superfluid state can not be thermodynamically stable. The various candidates for the pairing state in the $P \neq 0$ situation have been proposed, e.g., the Fulde-Ferrell-Larkin-Ovchinnikov (FFLO) modulated pairing state,^{11,12} the BCS-normal phase separation (PS),¹³ the breached pairing or the Sarma state,¹⁴ the deformed Fermi surface superfluid (DFS),^{15,16} the p -wave pairing state^{17,18} and so on. These proposed pairing states are robust even in the presence of the imbalanced spin density, i.e., the “magnetized” or imbalanced superfluid. The studies on the thermodynamic stability of such exotic pairing state has a long history.^{2,19}

Recently, the superfluid phase diagram for the homogeneous system has been extended to the BCS-BEC crossover regime by a number of authors.^{20–34} Here the phase diagram is constructed in a plane of the temperature T and the population imbalance P . According to

*E-mail address: mizushima@mp.okayama-u.ac.jp

them, there appears the PS in BEC side. In the further deep BEC limit, the homogeneous BEC superfluid of the boson-fermion mixture is favored.^{35,36} The FFLO state becomes thermodynamically stable in narrow window of the BCS side. Their studies take into account of only one particular form of the FFLO pairing, which has a single center-of-mass momentum vector \mathbf{Q} , i.e., $\Delta(\mathbf{r}) = \Delta_0 e^{i\mathbf{Q}\cdot\mathbf{r}}$. However it should be emphasized that for arbitrary P value, the oscillation of the stable FFLO phase can be described with the multiple vectors \mathbf{Q} and $-\mathbf{Q}$, i.e., $\Delta(\mathbf{r}) = \Delta_0 \cos(\mathbf{Q}\cdot\mathbf{r})$.^{12,37} This effect has not been considered in the previous works, and the generalized FFLO phase may be competitive with the PS in the remaining area of the phase diagram.^{32,38}

The presence of a trap potential which is used to capture an atomic gas in the actual experiment may lead to the different situation. The simplest way to take account of the trap is to employ the local density approximation (LDA), which is achieved by replacing the chemical potential to the local quantity including the trap potential. The LDA calculation^{39–47} predicts that the PS state, i.e., the BCS state surrounded by the spin polarized normal domain, is favored under the realistic situation with a large amount of particles and fully three dimensional trap. However, we should mention that the LDA eliminates the FFLO pairing state which is one of the possible candidates for the ground state, because of the lack of the gradual spatial variation of the pairing field. Including the gradient effect, the fully numerical analysis has been performed by several authors in the weak coupling BCS regime^{48–50} and at the unitary limit.^{51–53} They predict the stability of the FFLO oscillation which can not be described with a single \mathbf{Q} .

The aim of this paper is twofold: The first goal is to clarify the ground state of trapped fermions with population imbalance. Previously in our series of papers,^{48,49} we presented the numerical results in the weak coupling BCS regime. The current work covers the wider region including the BEC side of a resonance, in the plane of the population imbalance P and the dimensionless parameter $k_F a$, where k_F is the Fermi wave number. To address such a problem, we start with the Bogoliubov-de Gennes (BdG) equation⁵⁴ which takes the contribution from the gradient effect of the pairing field and describes the physics in the atomic scale $\sim k_F^{-1}$.

The second goal of the present paper is to discuss how the quasiparticle structure in the BCS-BEC crossover under population imbalance affects the radio-frequency (RF) spectroscopy which has been experimentally performed by Schunck *et al.*⁸

Also, we investigate how the situation with the large particle number $N = \mathcal{O}(10^5)$ changes the FFLO oscillation. Throughout this work, we fully solve the BdG equation coupled with the regularized gap equation and number equation, where the contributions from the higher energy are supplemented by the LDA. This hybrid calculation enables to demonstrate the stability of the FFLO modulation in the quantitative level, which is comparable with the recent experiments.^{3–8} The numerical results indicate that there exists the FFLO modulation even in the vicinity of a Feshbach resonance $1/k_F a \sim -0.5$ which

has been already realized by the experiment.⁵

This paper is organized as follows. In Sec. 2, we derive the BdG equation coupled with the regularized gap equation, based on the single channel model. Also, we show the numerical results on the $1/k_F a$ -dependence of basic physical quantities in the BCS-BEC crossover without population imbalance. We present the ground state structures of the imbalanced system in Sec. 3, where the spatial profiles of the pairing field and densities in the strongly interacting system ($1/k_F a < 1$) are displayed. In addition, we shall present a quantum phase diagram in a $1/k_F a$ - P plane. Section 4 presents the numerical results on the local density of states (LDOS) and the RF spectroscopy for the imbalanced superfluid in the BCS-BEC crossover. The final section is devoted to conclusions and discussions. In addition, we describe the supplemental information, e.g., the derivation of the thermal Green's function and the gap equation, in Appendices A and B.

2. Theoretical formulation: Single-channel model

2.1 Bogoliubov-de Gennes equation

Let us consider a Fermi gas distributed in two hyperfine spin states ($\sigma = \uparrow, \downarrow$). The Fermi system across a broad Feshbach resonance, which is realized in ^6Li or ^{40}K atoms, can be well described by the single-channel Hamiltonian:

$$\mathcal{H} = \int d\mathbf{r} \int d\mathbf{r}' \left[\sum_{\sigma} \psi_{\sigma}^{\dagger}(\mathbf{r}) H_{\sigma}^{(0)} \psi_{\sigma}(\mathbf{r}) \delta(\mathbf{r} - \mathbf{r}') + U(\mathbf{r} - \mathbf{r}') \psi_{\uparrow}^{\dagger}(\mathbf{r}) \psi_{\downarrow}^{\dagger}(\mathbf{r}') \psi_{\downarrow}(\mathbf{r}') \psi_{\uparrow}(\mathbf{r}) \right], \quad (2)$$

with the creation and annihilation operators of fermions, $\psi_{\sigma}^{\dagger}(\mathbf{r})$ and $\psi_{\sigma}(\mathbf{r})$. The single-particle Hamiltonian is given by

$$H_{\sigma}^{(0)}(\mathbf{r}) = -\frac{1}{2M} \nabla^2 + V(\mathbf{r}) - \mu_{\sigma}, \quad (3)$$

where the atoms with the mass M are trapped by a harmonic potential $V(\mathbf{r})$. Throughout this paper, we set $\hbar = k_B = 1$. The interatomic interaction potential is $U(\mathbf{r} - \mathbf{r}')$ and the chemical potential of two species is $\mu_{\uparrow, \downarrow} = \mu \pm \delta\mu$, where without the loss of generality, we put $\mu_{\uparrow} \geq \mu_{\downarrow}$, i.e., the spin-up (spin-down) is the majority (minority) component.

Following the procedure described in Appendix A, the Bogoliubov-de Gennes equation is given as

$$\begin{bmatrix} \mathcal{K}_{\uparrow}(\mathbf{r}) & \Delta(\mathbf{r}) \\ \Delta^*(\mathbf{r}) & -\mathcal{K}_{\downarrow}^*(\mathbf{r}) \end{bmatrix} \begin{bmatrix} u_{\nu}(\mathbf{r}) \\ v_{\nu}(\mathbf{r}) \end{bmatrix} = E_{\nu} \begin{bmatrix} u_{\nu}(\mathbf{r}) \\ v_{\nu}(\mathbf{r}) \end{bmatrix}, \quad (4)$$

where the diagonal element is obtained from $\mathcal{K}_{\sigma}(\mathbf{r}, \mathbf{r}') \equiv \delta(\mathbf{r} - \mathbf{r}') \mathcal{K}_{\sigma}(\mathbf{r})$ in Eq. (A.3b). This equation describes the quasiparticle state with eigenfunction $[u_{\nu}, v_{\nu}]$ and eigenenergy E_{ν} under the pairing field Δ and the Hartree potential $g\rho_{\sigma}$. Here, the interparticle interaction is characterized by the s -wave scattering, $U(\mathbf{r} - \mathbf{r}') = g\delta(\mathbf{r} - \mathbf{r}')$, whose “bare” coupling constant is $g = 4\pi a/M$ with the s -wave scattering length a . Hereafter, the interaction strength of the system is characterized with the dimensionless form $k_F a$ with the Fermi wave number $k_F \equiv \sqrt{2ME_F}$. E_F is the Fermi energy in a non-interacting

Fermi gas, whose definition is given in Sec. 2.2.

The “bare” coupling constant, however, carries two singular contributions to the BdG equation: (i) An ultra-violet (UV) divergence of the pair potential $\Delta(\mathbf{r})$ and (ii) the divergence of the Hartree potential at the unitary limit $k_F a \rightarrow \pm\infty$. It is known^{55–57} that the UV divergence can be renormalized by replacing the bare coupling constant g to the effective one $\tilde{g}(\mathbf{r})$ in the gap equation. The explicit form of the regularized gap equation^{58, 59} is given as

$$\Delta(\mathbf{r}) = \tilde{g}(\mathbf{r}) \sum_{\nu} u_{\nu}(\mathbf{r}) v_{\nu}^*(\mathbf{r}) f_{\nu}, \quad (5)$$

where the renormalized coupling constant $\tilde{g}(\mathbf{r})$ is given by,

$$\frac{1}{\tilde{g}(\mathbf{r})} = \frac{1}{g} + \frac{M k_c(\mathbf{r})}{2\pi^2} \left[1 - \frac{k_F(\mathbf{r})}{2k_c(\mathbf{r})} \ln \frac{k_c(\mathbf{r}) + k_F(\mathbf{r})}{k_c(\mathbf{r}) - k_F(\mathbf{r})} \right]. \quad (6)$$

Here the Fermi distribution function is $f_{\nu} \equiv f(E_{\nu}) = 1/(e^{E_{\nu}/T} + 1)$. The sum in the final expression of the gap equation (5) is done for all the eigenstates with both positive and negative eigenenergies, whose details are described in Appendix A. The above gap equation (5) is now free from the energy cutoff E_c . For $E_c \gg E_F$, the expression for $\tilde{g}(\mathbf{r})$ coincides with that obtained from the two-body T -matrix in the absence of the medium.⁵⁵ Here, $k_F(\mathbf{r})$ and $k_c(\mathbf{r})$ are the local wave vectors defined by the local Fermi and cutoff energies, respectively:

$$E_F(\mathbf{r}) = \mu - V(\mathbf{r}), \quad (7a)$$

$$E_c(\mathbf{r}) = \frac{k_c^2(\mathbf{r})}{2M} + V(\mathbf{r}) - \mu. \quad (7b)$$

Note that even if the gap equation with the bare coupling constant g is singular, the effective one $\tilde{g}(\mathbf{r})$ yields the non-singular value with the negative sign in the extensive region, ranging from unitary limit to the deep BEC limit.

As for the second divergent behavior (ii), it is known^{60, 61} that the divergent term at unitary limit can be renormalized if we consider the many body contributions beyond the mean-field self-energy, where the system behaves like the Fermi liquid with the effective mass. Hence, we remove the singularity by neglecting the Hartree term, that is, the diagonal elements in the BdG equation (4) is replaced to the single-particle Hamiltonian in Eq. (3): $\mathcal{K}_{\sigma}(\mathbf{r}) = H_{\sigma}^{(0)}(\mathbf{r})$.

In summary, the renormalized coupling constant in Eq. (6) and the neglect of the Hartree potential lead to the regularization of the BdG formalism. The BdG equation (4) is self-consistently coupled with the gap equation (5) and number equation

$$N = \sum_{\sigma} N_{\sigma} = \int d\mathbf{r} \sum_{\sigma} \rho_{\sigma}(\mathbf{r}), \quad (8)$$

where the particle density in each spin state is given from Eqs. (A.4b) and (A.5) by

$$\rho_{\uparrow}(\mathbf{r}) = \sum_{\nu} |u_{\nu}(\mathbf{r})|^2 f_{\nu}, \quad (9a)$$

$$\rho_{\downarrow}(\mathbf{r}) = \sum_{\nu} |v_{\nu}(\mathbf{r})|^2 (1 - f_{\nu}). \quad (9b)$$

This formalism is now free from any divergence and provides the qualitative expression for strongly interacting Fermi systems in the BCS-BEC crossover.⁶² Note that this equation within the single-channel model gives equivalent results with the another mean-field theory based on the fermion-boson model, in the case of a broad resonance.⁶³ Also, we would like to mention that in the deep BEC limit ($1/k_F a \rightarrow +\infty$), the BdG equation (4) can be mapped to the Gross-Pitaevskii equation with the small parameter $\Delta/|\mu|$,⁶⁴ where Δ describes the wave function of the condensed molecular bosons. As we shall show later, the chemical potential at the unitary limit $1/k_F a \rightarrow 0$ is estimated as $\mu/E_F = 1 + \beta$ with $\beta = -0.4$ in the current theory, which is comparable with the recent experimental results $\beta = -0.54$.^{65, 66}

In performing the numerical calculation, we compute the gap equation (5) with the following twofold procedure: $\Delta(\mathbf{r}) = \Delta_{\text{BdG}}(\mathbf{r}) + \Delta_{\text{LDA}}(\mathbf{r})$. The first term is composed of the contributions from low-energy eigenstates $|E_{\nu}| < E_c^{(\text{BdG})}$ obtained from the exact diagonalization of the BdG equation (4). The quantity Δ_{LDA} with the higher energy contribution above $E_c^{(\text{BdG})} < E_{\nu} < E_c$ is supplemented by the LDA, whose explicit expression is given by

$$\Delta_{\text{LDA}}(\mathbf{r}) = \tilde{g}(\mathbf{r}) \int_{p_c^{(\text{BdG})}}^{\infty} \frac{d\mathbf{p}}{(2\pi)^3} \frac{\Delta(\mathbf{r})}{2E(\mathbf{p}, \mathbf{r})} \times [f(E_{\uparrow}(\mathbf{p}, \mathbf{r})) + f(E_{\downarrow}(\mathbf{p}, \mathbf{r})) - 1], \quad (10)$$

with $p_c^{(\text{BdG})} \equiv \sqrt{2ME_c^{(\text{BdG})}}$. Here, we set $E_{\uparrow, \downarrow}(\mathbf{p}, \mathbf{r}) = E(\mathbf{p}, \mathbf{r}) \mp \delta\mu$ with $E(\mathbf{p}, \mathbf{r}) = \sqrt{[\epsilon(\mathbf{p}, \mathbf{r})]^2 + |\Delta(\mathbf{r})|^2}$, $\epsilon(\mathbf{p}, \mathbf{r}) = p^2/2m - \mu$, and $E_c = p_c^2/2m - \mu$. Also, the high energy contribution to each spin density is expressed within the LDA as $\rho = \rho_{\sigma}^{(\text{BdG})} + \rho_{\sigma}^{(\text{LDA})}$ with

$$\rho_{\uparrow, \downarrow}^{(\text{LDA})}(\mathbf{r}) = \frac{1}{2} \int_{p_c^{(\text{BdG})}}^{\infty} \frac{d\mathbf{p}}{(2\pi)^3} \left[\left\{ 1 + \frac{\epsilon(\mathbf{p}, \mathbf{r})}{E(\mathbf{p}, \mathbf{r})} \right\} \times f(E_{\uparrow, \downarrow}(\mathbf{p}, \mathbf{r})) + \left\{ 1 - \frac{\epsilon(\mathbf{p}, \mathbf{r})}{E(\mathbf{p}, \mathbf{r})} \right\} f(-E_{\downarrow, \uparrow}(\mathbf{p}, \mathbf{r})) \right]. \quad (11)$$

We should mention that the spatial variation of the pairing field is mainly determined by the contributions from the eigenstates with the energy close to the Fermi energy, while the eigenstates with the higher energy may be described within the semiclassical approximation, i.e., the LDA. This hybrid procedure has also been used in the numerical analysis of the thermodynamic quantities at the unitary limit.⁵¹

2.2 Calculated system

We numerically solve the BdG equation (4) self-consistently coupled with the gap equation (5). The theory takes account of a trap potential and the mismatch of Fermi surfaces $\delta\mu \equiv (\mu_{\uparrow} - \mu_{\downarrow})/2$. At each iteration step, the chemical potential μ is adjusted to fix the total particle number defined in Eq. (8). In the current work, we consider a cylindrical symmetric system with a trap potential $V(\mathbf{r}) = \frac{1}{2} M \omega^2 r^2$ ($r^2 = x^2 + y^2$), imposing a periodic

boundary condition with the periodicity $Z = 3d$ ($d^{-1} \equiv \sqrt{M\omega}$) along the z -direction. Under such cylindrical symmetry, the quasiparticle wave functions are written as $u_\nu(\mathbf{r}) = u_\nu(r)e^{i(q_\theta\theta + q_z z)}$ and $v_\nu(\mathbf{r}) = v_\nu(r)e^{i(q_\theta\theta + q_z z)}$ with the quantum number along the azimuthal- and z -axis: $q_\theta = 0, \pm 1, \pm 2, \dots$ and $q_z = 0, \pm 2\pi/Z, \pm 4\pi/Z, \dots$.

The BdG matrix in Eq. (4), then, is transformed by spatial discretization into a banded matrix with respect to the radial axis, which can be solved by using the Lanczos/Arnoldi algorithm implemented in the ARPACK libraries.⁶⁷ Throughout this paper, we choose the total particle number as $N = 3,000$ and $150,000$. The corresponding Fermi energies in $\Delta = 0$ are given as $E_F = 32\omega$ and 154ω , respectively, by using the definition $E_F/\omega = (30\pi n_z/16)^{2/5}$ with $n_z \equiv N/Z$. Throughout this paper, we set $E_c^{(\text{BdG})} = 150\omega = 4.7E_F$ for the case of $N = 3,000$ atoms and $E_c^{(\text{BdG})} = 200\omega = 1.3E_F$ for $N = 150,000$ because of the limitation of computation times. However, the higher energy contributions up to $E_c = 1000\omega$ is supplemented within the LDA, shown in Eqs. (10) and (11).

2.3 Calculations for balanced systems

Before going into the numerical results in superfluid states with population imbalance, let us present the basic properties in balanced superfluids, described within

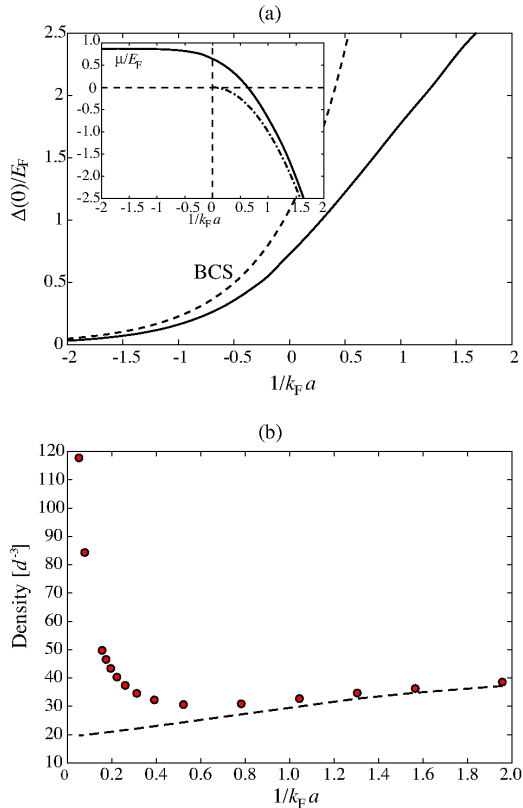


Fig. 1. (a) Maximum values of pairing amplitude in equal mixture $P = 0$ at $T = 0$ and $N = 3,000$ as a function of $1/k_F a$. The dashed line is the BCS form described in the text. The inset displays the chemical potential shift. The dash-dotted line corresponds to one half of the binding energy $E_b/2E_F$. (b) The “order parameter for molecular bosons” $2|\Psi_{\text{BEC}}(r=0)|^2$ (circles) is compared with the total density $\rho(r=0)$ (dashed line). The definition for Ψ_{BEC} is described in the text.

the above mean-field theory. First, in Fig. 1(a), we show the pairing amplitude Δ_0/E_F as a function of $1/k_F a$ where Δ_0 is the maximum value of the pairing field at zero temperatures. It is found that in weak coupling limit $1/k_F a < -1$, the pairing field can be asymptotically described with the standard BCS relation, $\Delta_0/E_F = 8e^{-2-\pi/k_F|a|}$, while the pairing in the opposite limit turns to the wave function of tightly bound molecular bosons, i.e., the order parameter of BEC. In this BEC limit, it is known that the BdG equation in the single-channel model can be mapped into the Gross-Pitaevskii equation for molecular bosons⁶⁴ where the fermionic chemical potential goes to one half of the binding energy of pairs $E_b/E_F = -2/(k_F a)^2$, shown in the inset of Fig. 1(a). The order parameter of molecular bosons is expressed as $\Psi_{\text{BEC}}(\mathbf{r}) = \sqrt{\frac{M^2 a}{8\pi}} \Delta(\mathbf{r})$, corresponding to the total fermionic density $2|\Psi_{\text{BEC}}(\mathbf{r})|^2 = \rho(\mathbf{r})$. As shown in Fig. 1(b), this asymptotic behavior can be confirmed in the direct calculation of the BdG equation.

The intermediate region nearby $1/k_F a = 0$ is smoothly connected from the BCS to BEC limits. Then, the pairing field Δ obtained from the single-channel model describes the order parameter composed of the fermionic pairs and the wave function of the molecular BEC. The pairing amplitude at the unitary limit is $\Delta_0/E_F = 0.7$, which is overestimated in comparison with $\Delta_0/E_F = 0.5$ in the strong coupling theory.^{68,69} It is also found that the coherence length is saturated toward the length scale of the inter-atomic spacing $\xi_0 k_F = 2E_F/\Delta_0 = \mathcal{O}(1)$ as $k_F a$ approaches the BEC limit $1/k_F a \rightarrow \infty$.

3. Ground states in the imbalanced system at $T = 0$

3.1 Superfluid states in weak-coupling BCS regime

We now consider imbalanced $N = 3,000$ fermions trapped by a cylindrical potential at $T = 0$. Figure 2(a) shows the spatial profile of the pairing field at $P = 0$ (dashed line) and $P = 0.4$ (solid line) in the weak coupling BCS side of a resonance, $1/k_F a = -0.52$. With this coupling constant, it is found that the quantum phase transition from the superfluid to normal states is induced at the critical population imbalance $P_c = 0.61$. It is seen from Fig. 2(a) that in the central region labeled as (I), the population imbalance does not affect the pairing field. In contrast, the superfluid pairing field is quenched in the most outside region labeled as (III). The pairing field in the intermediate region (II) yields the spatial oscillation, i.e., the FFLO modulation, where the amplitude gradually decreases toward the edge of the cloud.

These characteristics in $\Delta(r)$ are reflected by the density profiles of each spin component displayed in Fig. 2(b), where we define the local population difference, called the local “magnetization”, as

$$m(\mathbf{r}) \equiv \rho_\uparrow(\mathbf{r}) - \rho_\downarrow(\mathbf{r}). \quad (12)$$

Each spin state in the region (I) attracts each other where the magnetization is excluded in order to fully gain the condensation energy. In the intermediate region (II) the gap function changes its sign, allowing to accommodate the excess majority species. This is indeed characteristic

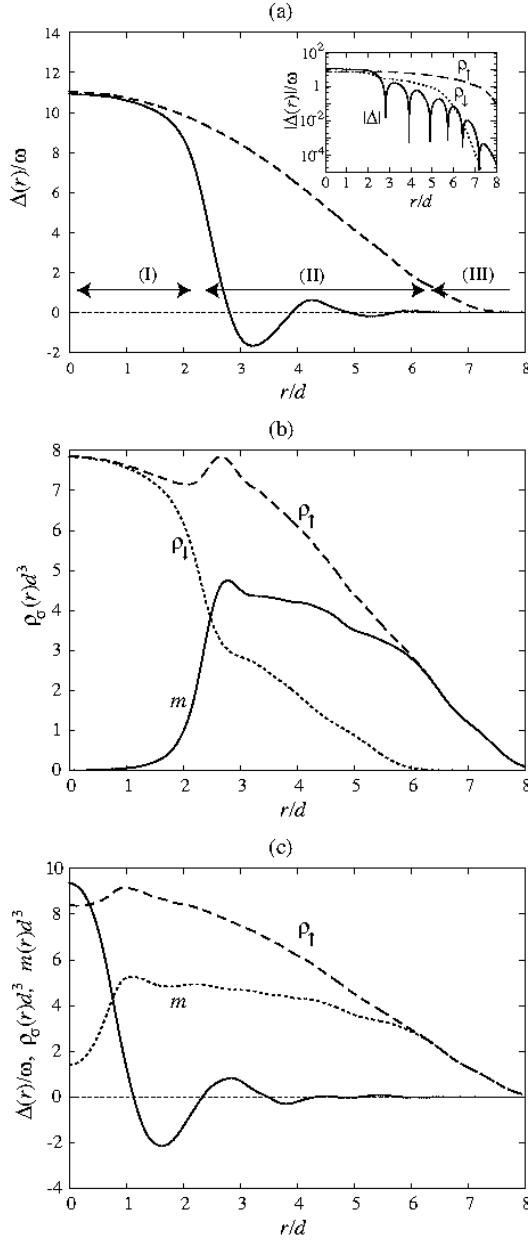


Fig. 2. Spatial profiles of (a) the pairing field at $P=0$ (dashed line) and $P=0.48$ (solid line) and (b) the corresponding density profiles where the dashed, dotted, and solid lines denote the majority and minority densities and the local magnetization, respectively. The inset in (a) shows $\Delta(r)$ (solid line) and $\rho_\sigma(r)$ (dashed and dotted lines) with the logarithmic scale. In (c), $\Delta(r)$, $m(r)$, and $\rho_\uparrow(r)$ at $P=0.58$ are displayed with solid, dotted, and dashed lines. All results are at $T=0$ and $1/k_F a = -0.52$.

in the FFLO state; The accumulation of excess majority species at $T=0$ results from the topological structure of $\Delta(r)$. The quasiparticles across the FFLO node experience the π -phase shift of the pair potential, allowing to form the mid-gap state spatially bound there, called the Andreev bound state in more general context.^{37,70,71} The energy of this state is situated in the middle of the energy gap and the mismatch of the Fermi surface causes the difference of the occupation of this bound state, leading to the local “magnetization” around the nodes, as seen in Fig. 2(b). Here, there remains a sufficient amount

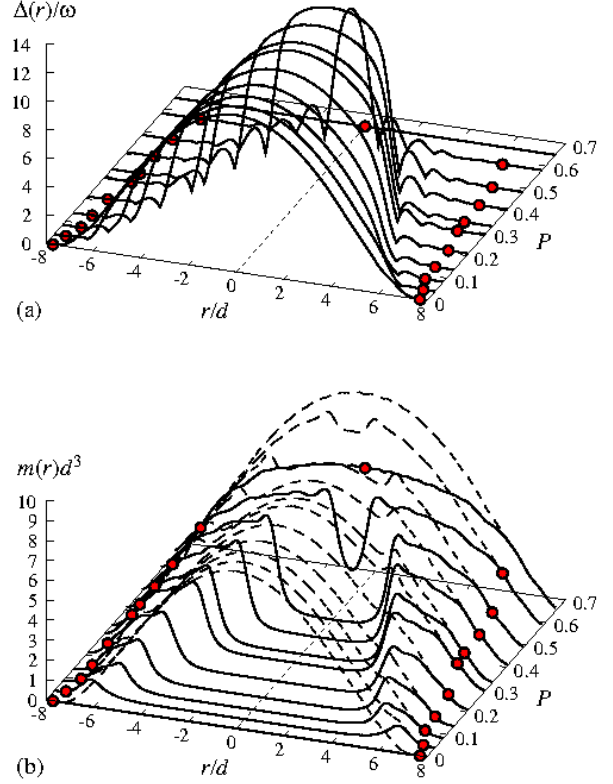


Fig. 3. The spatial distribution of $|\Delta(r)|$ at $1/k_F a = -0.52$ and $T=0$ is shown in (a) for various P 's. In (b), the corresponding local magnetization $m(r)$ (solid lines) and the majority density $\rho_\uparrow(r)$ (dashed lines) are displayed. The circles correspond to the radii of the pairing field, R_c defined as $\Delta(R_c)/\Delta_0 = 10^{-3}$.

of the minority component for the pairing with the majority one, i.e., the local magnetization is not fully polarized. These features are revealed by the bimodal distribution in the minority component (see around $r/d \sim 3$ in Fig. 2(b)).

Figure 2(c) shows the gap and density profiles in the vicinity of the critical population imbalance $P/P_c = 0.95$. In this situation, the local magnetic moment $m(r)$ governs the entire region of the system, where the “empty core” in the central region of local magnetization vanishes. This leads to the quench of the balanced BCS pairing even at $r \sim 0$. As seen Fig. 2(c), however, the superfluidity is still robust up to the edge of the minority component $r \sim 6.5d$ by entirely forming the FFLO pairing, accompanied with the partially polarized spins.

In Fig. 3 we display the P -dependence of the pairing field and local magnetization at $T=0$ and $1/k_F a = -0.52$. With increasing P , the oscillating region becomes wider towards the central region, while the radii of the pairing field R_c keep the constant value $R_c/d \sim 7$ up to the critical population imbalance $P_c = 0.61$. This FFLO pairing state is not describable with the LDA where the “superfluidity” is localized in the central region (I) and the surroundings in (II) and (III) are regarded as the normal state, i.e., the BCS-normal PS state.^{39–41,43} It is found that this oscillating pairing state becomes robust up to the critical population imbalance $P_c = 0.6$ at $T=0$ and

$1/k_F a = -0.52$, only the equal population $P = 0$ is the stable situation for the non-oscillating BCS state. Beyond P_c , the superfluid state turns into the normal state through the second-order phase transition.

In the outside region of R_c , in which the gap is almost vanishing, the complete spin-polarized state is attained. It should be emphasized again that the central region $r \sim 0$, in which the magnetization is completely excluded, catches the clear signature of the “balanced” superfluidity, while the surrounding area with the partially polarized spins also keeps superfluidity composed of the “imbalanced” FFLO pairing.

3.2 Strong coupling region: From unitary limit to BEC regime

Let us now consider the strong coupling BEC region. The pairing field in the BEC side of a resonance is completely different from that in the BCS side. Figure 4 shows the spatial profiles of $\Delta(r)$, $\rho_\sigma(r)$, and $m(r)$ at $1/k_F a = 0.52$, $P = 0.73$, and $T = 0$. The superfluid pairing state is still robust in the central region of the system, while the outside region turns to the normal states. The intermediate region (II) smoothly connects the superfluid core (I) and the normal state (III) without any

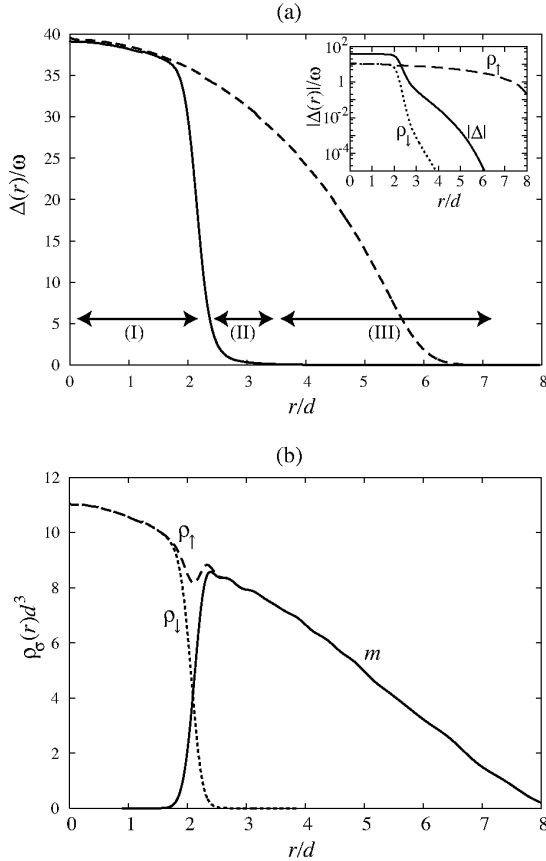


Fig. 4. Spatial profiles of (a) the pairing field at $P = 0$ (dashed line) and $P = 0.73$ (solid line) and (b) the corresponding density profiles where the dashed, dotted, and solid lines denote the majority and minority densities and the local magnetization, respectively. The inset in (a) shows $\Delta(r)$ (solid line) and $\rho_\sigma(r)$ (dashed and dotted lines) with the logarithmic scale. All results are at $T = 0$ and the BEC side $1/k_F a = +0.52$.

spatial oscillation of the pairing. In contrast with the BCS side shown in Fig. 2, it is seen from the inset of Fig. 4(a) that its intensity exponentially decays toward the edge of the minority component. As seen in Fig. 4(b), the magnetization is completely excluded from the central region (I), while the spins in the outer region (III) are fully polarized. In the strong coupling regime, the intermediate region (II) plays a role as the domain wall between the superfluid core (I) and fully polarized normal state (III). This phase-separated profile is commonly seen in the other theoretical calculations based on the LDA,^{39–44,46,47} except for the proximity effect of the pairing field in the vicinity of the domain wall.

Figure 5 displays the spatial distributions of the pairing field and the local magnetization as a function of P , where the circles denote the edge of the pairing field R_c defined as $\Delta(R_c)/\Delta_0 = 10^{-3}$. In the BEC side, the critical population imbalance is uniquely determined as $P_c = 1$ at zero temperatures. The robustness of the superfluidity is supported by the fact that the superfluidity is realized by the formation of the pair in local, i.e., molecules.

Also, as for the P -dependence of the ground state shown in Fig. 5, there exist two clear differences between the BEC and BCS regimes; First, in the case of $1/k_F a = 0.52$, the radii of the condensation area R_c gradually shrinks as P approaches $P_c = 1$, while R_c in the BCS regime has the almost fixed value up to P_c . Second, the domain composed of the “fully” polarized spins

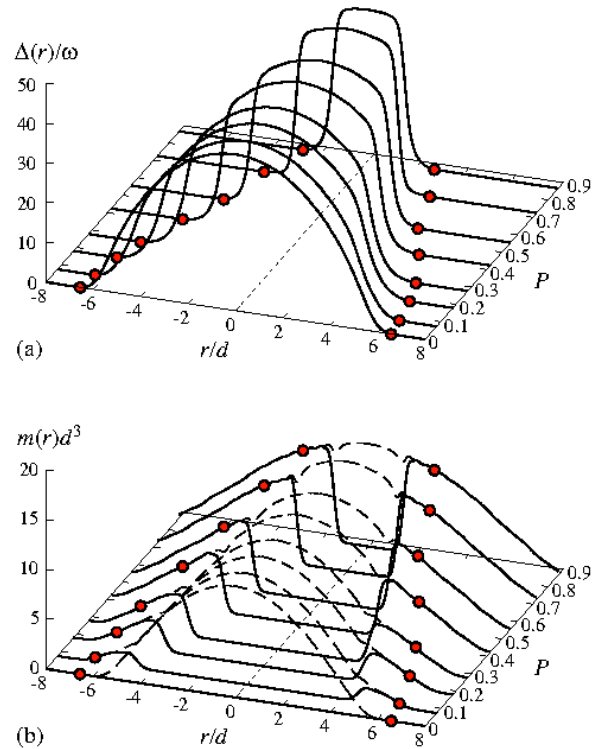


Fig. 5. The spatial distribution of $|\Delta(r)|$ at the BEC side $1/k_F a = 0.52$ and $T = 0$ is shown in (a) for various P 's. In (b), the corresponding local magnetization $m(r)$ (solid lines) and the majority density $\rho_\uparrow(r)$ (dashed lines) are displayed. The circles correspond to the edge of the pairing field R_c defined as $\Delta(R_c)/\Delta_0 = 10^{-3}$.

grows up around the empty core in all P 's of the BEC side. In contrast, as seen in Fig. 3, the outside area in the BCS side has enough region (II) which is composed of the “partially” polarized spins and the minority spins take a part in the superfluid pairing with the majority spins.

The pairing field and density profiles at the unitary limit are displayed in Fig. 6 where there remains the FFLO oscillation in the outside area of the “core” having the balanced spin density. This modulation survives as the proximity effect between the balanced superfluid and the fully polarized domains, analogous to the superconductor/ferromagnet interfaces.⁷² Note that the periodicity of the FFLO oscillation may be scaled with the coherence length ξ_0 . As shown in the inset of Fig. 6, the FFLO oscillation is completely periodic with the periodicity $L \sim d$, which is comparable with $\xi_0 = 2.5k_F^{-1} = 0.31d$, i.e., $L \sim 3\xi_0$. In the BCS side $k_F a = -0.52$, the FFLO modulation region (II), which becomes wider toward the edge of the cloud, has the longer periodicity $L \sim 2d = 2.7\xi_0$, e.g., see Fig. 2, where $\xi_0 = 6k_F^{-1} = 0.75d$. In contrast, the coherence length saturates to the interparticle spacing, $\xi_0 \sim k_F^{-1}$, in BEC side, in which the oscillation suddenly vanishes. The resulting density profile shown in

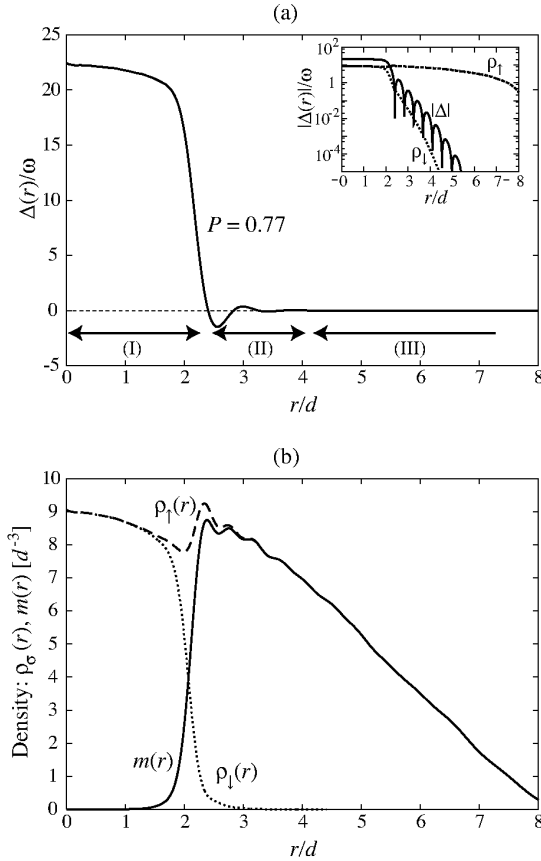


Fig. 6. Spatial profiles of (a) the pairing field and (b) the corresponding density profiles at $P = 0.77$ and the unitary limit $1/k_F a = 0$. In (b), the dashed, dotted, and solid lines denote the majority and minority densities and the local magnetization, respectively. The inset in (a) shows $\Delta(r)$ (solid line) and $\rho_\sigma(r)$ (dashed and dotted lines) with the logarithmic scale. All results are at $T = 0$.

Fig. 6(b) is almost unchanged with that in the BEC side (See Fig. 4), namely, yielding the phase separation. This is quite different from that in the BCS side shown in Fig. 2(b).

3.3 Large N system

We now turn to a situation with the realistic particle number $N = 150,000$. The spatial profiles of the pairing field and densities at $1/k_F a = -1.2$, -0.7 , and at the vicinity of the unitary limit $1/k_F a = -0.14$ are displayed in Fig. 7 and in Fig. 8, respectively. The tendency due to the FFLO pairing, which has been already seen in the system with $N = 3,000$ atoms, is commonly reproduced even in the large N system. For instance, the outside region $r \geq 8d$ of Fig. 7 shows that the pairing field yields the FFLO oscillation, whose indirect signature in the macroscopic quantity is the partially polarized spin density. Note that the recent experiments⁵ have been performed in the wide $k_F a$ range, $1/k_F |a| \leq 0.5$, in which the FFLO modulation survives. The periodicity L of the oscillation in Fig. 8(a) is the larger length scale than the interparticle spacing, $L \sim 4d = 70k_F^{-1}$, which is comparable with the coherence length ξ_0 , $L = 3.3\xi_0$ with $\xi_0 = 21k_F^{-1}$ and $k_F^{-1} = 0.06d$.

The spatial profiles in the strong coupling regime are shown in Fig. 8. The local “magnetization” is in good

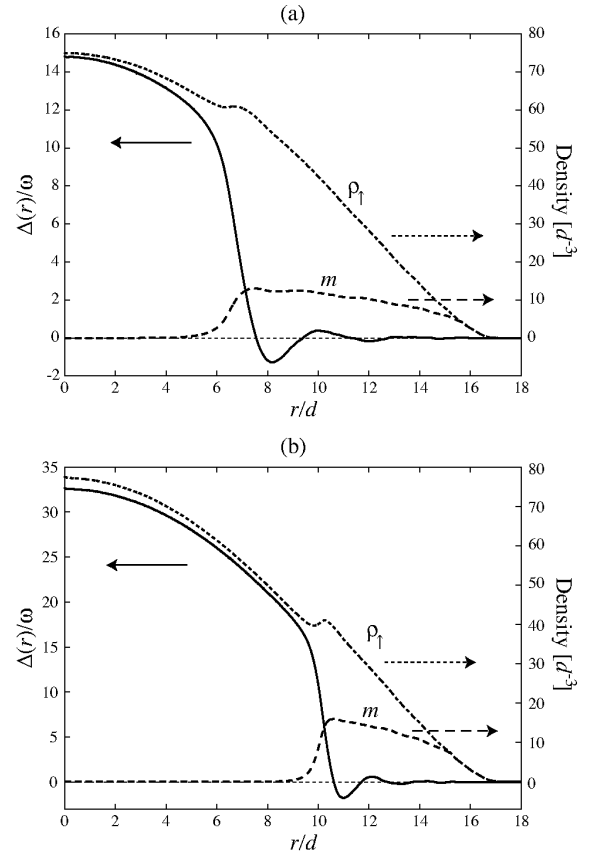


Fig. 7. Spatial profiles of the pairing field (solid line), the majority spin density (dotted line) and the local magnetization (dashed line) in the system with $N = 150,000$ at $1/k_F a = -1.2$ and $P = 0.13$ (a) and $1/k_F a = -0.7$ and $P = 0.12$ (b). All results are at $T = 0$.

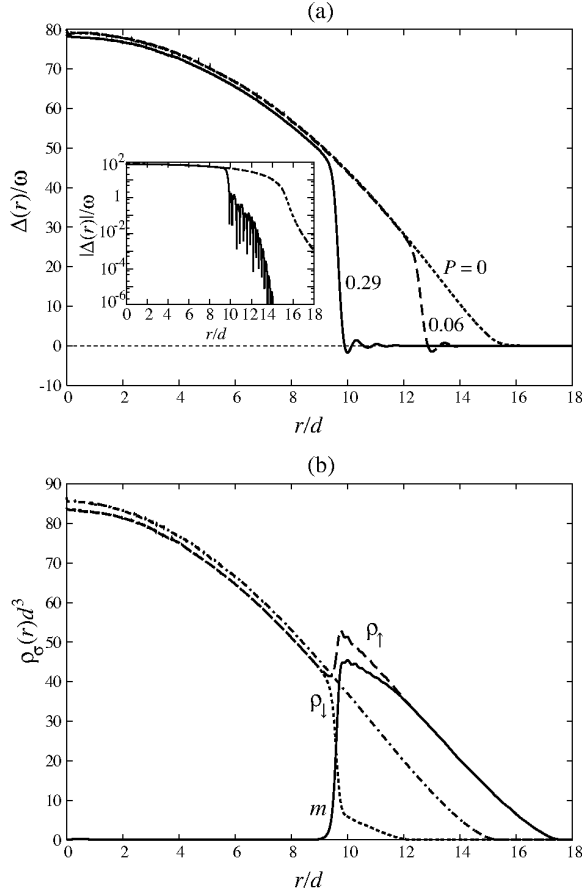


Fig. 8. Spatial profiles of the pairing field (a) and the density (b) in the system with $N = 150,000$ at $1/k_F a = -0.14$ and $T = 0$. The dotted, dashed, and solid lines in (a) show the pairing field at $P = 0, 0.06$, and 0.29 , respectively. Also, those in (b) denote the minority and majority densities, and the local magnetization, respectively. The dot-dashed line in (b) correspond to the density for the up spins at $P = 0$. In the inset of (a), $|\Delta(r)|$ at $P = 0$ (dotted line) and 0.29 (solid line) is displayed with the logarithmic scale.

agreement with the experiment which has been observed by using the phase-contrast imaging and 3D image reconstruction.⁷ While the local magnetization yields the PS like profile, there exists the FFLO modulation in the pairing field. In this strong coupling regime $1/k_F a = -0.14$, the periodicity of the FFLO oscillation becomes shorter, which is comparable with the interparticle spacing $L \sim 0.6d \sim 10.5k_F^{-1}$ and its intensity exponentially decay as seen in the inset of Fig. 8(a). With $\xi_0 = 3.7k_F^{-1}$, the oscillation period is scaled as $L \sim 2.8\xi_0$.

In summary, through the extensive range of the interaction $k_F a < 0$, the oscillation periodicity L is well scaled with the coherence length ξ_0 as $L = \alpha\xi_0$. The coefficient α is around 3. We also find that this result is insensitive to the total particle number, i.e., the Fermi wave length k_F^{-1} . Surprisingly, it is found that the period is almost unchanged against the increase of the population imbalance. The one example is displayed in Fig. 3(a), where inter-node spacing is almost fixed in the entire P 's. Note that since the FFLO oscillation periodicity in the absence of the trap potential is sensitive to the population

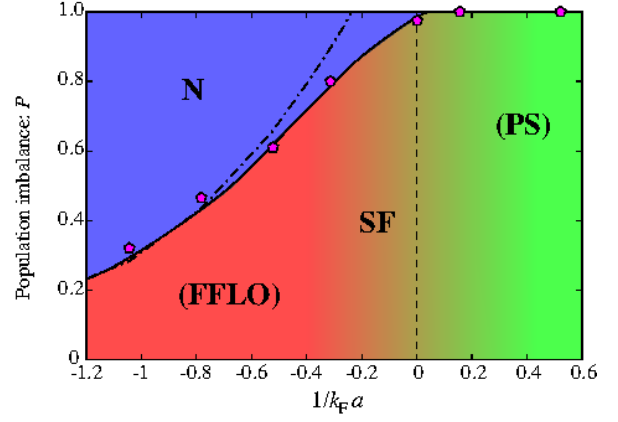


Fig. 9. (color online) Quantum phase diagram in a $1/k_F a$ - P plane. The points denote the estimated phase boundary between the superfluid (SF) and normal (N) phases. The pairing field in the superfluid phase exhibits the spatial oscillation (non-oscillation) in the negative (positive) $1/k_F a$. The dashed-dotted line is the extrapolation from the results of the weak coupling limit, $P_c = 1.9\Delta_0/E_F$,⁴⁹ where Δ_0 is the maximum intensity of $\Delta(r)$ at $T = 0$ and $P = 0$.

imbalance or alternatively the mismatch of the Fermi surface,^{37,48} the constancy of L may be peculiar to the finite trap system.

3.4 Quantum phase diagram

Let us now summarize the ground state of the imbalanced Fermi system in the BCS-BEC crossover by constructing the phase diagram at zero temperatures. Figure 9 shows the phase diagram in a plane of the dimensionless coupling constant $k_F a$ versus the population imbalance P for the system with the total atoms $N = 3,000$. It is important to mention that the critical population imbalance in the weak coupling limit $1/k_F a < -1$ exponentially depends on $1/k_F a$, i.e., $P_c \propto e^{-\pi/2k_F|a|}$, which means the linear behavior on the intensity of the pairing field, i.e., $P_c \propto \frac{\Delta_0}{E_F}$. In our previous work,⁴⁹ we found $P_c = 1.9\frac{\Delta_0}{E_F}$. In Fig. 9, the corresponding exponential line is depicted with Δ_0/E_F where Δ_0 is the maximum gap $\Delta(r=0)$ at $T = 0$ and $P = 0$. It is seen that this tendency is also confirmed in the current phase diagram obtained from the crossover theory. The superfluid phase below P_c at $k_F a < 0$ yields the spatial oscillation of the pairing, i.e., the FFLO state. The formation of the FFLO pairing pushes up the phase boundary, compared with the Pauli limit (See also Fig. 13).

The behavior of the P_c curve in the BEC side is contrast with that in the BCS side, where the phase boundary is uniquely determined as $P_c = 1$. This results from the fact that the superfluidity survives by locally forming the molecular-like pairing with the corresponding amount of majority spins. The SF phase at $1/k_F a > 0$ corresponds to the PS state without any oscillation of the pairing. The distinct phase boundary between the FFLO and PS states can not be defined because the FFLO state continuously turns into the PS state via the proximity effect in the BCS/polarized-normal domain interfaces, as has been discussed above. This is peculiar to the finite

trap system.

It has been proposed^{35,36} that as $1/k_F a$ goes to the deep BEC limit $1/k_F a \gg 1$, the PS state turns into the “homogeneous” imbalanced superfluid without the phase-separated domain, that is, the mixture system of the bosons and the spinless fermions is attained.

4. Quasiparticle structure and radio-frequency spectroscopy

4.1 Local density of states

The local density of states (LDOS) for each spin component is given by the definition,

$$\mathcal{N}_\sigma(r, E) = -\frac{1}{\pi} \Im \mathcal{G}_\sigma(\mathbf{r}\mathbf{r}, i\omega_n \rightarrow E + i\eta), \quad (13)$$

where $\mathcal{G}_\uparrow(\mathbf{r}\mathbf{r}', i\omega_n) = \mathcal{G}_{11}(\mathbf{r}\mathbf{r}', i\omega_n)$ and $\mathcal{G}_\downarrow(\mathbf{r}\mathbf{r}', i\omega_n) = -\mathcal{G}_{22}(\mathbf{r}\mathbf{r}', -i\omega_n)$. With the thermal Green’s function \mathcal{G}_{ij} described in Appendix B, one can read the LDOS for the spin-up state,

$$\mathcal{N}_\uparrow(r, E) = \sum_\nu |u_\nu(r)|^2 \delta(E - E_\nu), \quad (14a)$$

and for the spin-down state,

$$\mathcal{N}_\downarrow(r, E) = \sum_\nu |v_\nu(r)|^2 \delta(E + E_\nu). \quad (14b)$$

The LDOS’s for majority spin states in the BCS side are displayed in the top row of Fig. 10. In the balanced case, the low-lying excitations are bound in the surface of the cloud ($r \geq 4d$). It is known^{73,74} that the quasiparticles around the surface experience the effective potential composed of the trap potential $V(r) \propto r^2$ and the pair potential $\Delta(r)$, where the latter is the monotonic decrease function in the surface region. This may be reduced to the problem on quasiparticles confined in the quantum well like potential $\Delta(r) + V(r)$. Hence, the eigenenergies close to the Fermi level are discretized with the trap unit, i.e., there exists the finite small energy gap with $\mathcal{O}(\omega)$. In the finite P , however, the FFLO oscillation induces the mid-gap mode with the zero energy and the surface excitation gap vanishes as P increases. The quasiparticle around the FFLO node behaves like gapless normal particle, but the superfluidity survives.

Note that the LDOS profile for the minority species is almost same as that for the majority spins, except that the shift of the Fermi level, which is shifted downward $2\delta\mu$.

The bottom row in Fig. 10 shows the LDOS in the BEC side. At $1/k_F a = 0.52$, the maximum value of the energy gap is comparable with the Fermi energy $|\Delta_0| \sim E_F$. In contrast, the quasiparticle structure in the surface region is different from that of the BCS side. In the further deep BEC limit, the low-lying excitation can be characterized by the binding energy, that is, $E_{\mathbf{q}} = \sqrt{\mu^2 + \Delta^2} \sim |\mu|$. Also, the quasiparticle states in the energy band lower than $-\Delta(r) - \delta\mu$ are no longer the eigenstates of the harmonic oscillator, compared with that in the weak coupling $1/k_F a = -0.52$. With increasing P , as shown in the bottom row of Fig. 10, the particles, for instance, in $r/d > 4$ at $P = 0.56$, locally dissociate from the pairing state which turns to the normal state.

4.2 Basic formalism for radio-frequency spectroscopy

The spatially averaged quantity of the LDOS is observable in the radio-frequency (RF) spectroscopy which has been recently developed by several experimental groups in an equal mixture^{75–78} and an imbalanced system.⁸ The theoretical efforts have been performed by a number of authors based on the linear response^{73,79–83} and non-linear response theory.^{52,84} Here, following their previous works within the linear response theory, we describe the formulation for the RF spectroscopy in the imbalanced system.

We consider the another internal states $|e\rangle$ in addition to the two hyperfine states $|\sigma = \uparrow, \downarrow\rangle$ which forms a pairing via an effectively attractive interaction. The state $|e\rangle$ can be described by the field operator $\psi_e(\mathbf{r})$ and $\psi_e^\dagger(\mathbf{r})$, which obeys the standard fermionic commutation relation and is commutative with that of the other internal states. Following several works,^{73,79–83,85} we extend the original Hamiltonian describing the state $|\sigma\rangle$ to

$$\tilde{\mathcal{H}} = \mathcal{H}_{\text{MF}} + \mathcal{H}_e + \mathcal{H}_T + \frac{\omega_{\text{det}}}{2} \left[\sum_\sigma \mathcal{N}_\sigma - \mathcal{N}_e \right], \quad (15)$$

with

$$\mathcal{N}_\alpha = \int d\mathbf{r} \psi_\alpha^\dagger(\mathbf{r}) \psi_\alpha(\mathbf{r}), \quad \alpha = \sigma, e. \quad (16)$$

The Hamiltonian includes the following contributions; First, the Hamiltonian for atoms in the e state is given by

$$\mathcal{H}_e = \int d\mathbf{r} \psi_e^\dagger(\mathbf{r}) \left[H_e^{(0)} + \sum g_{e\sigma} \rho_\sigma(\mathbf{r}) \right] \psi_e(\mathbf{r}). \quad (17)$$

with $\mathcal{H}_e = -\frac{\nabla^2}{2M} + V(\mathbf{r}) - \mu_e$. Second, the Hamiltonian describing the “tunneling current” between internal states is introduced as

$$\mathcal{H}_T^{(\sigma)} = \int d\mathbf{r} \left[\Omega(\mathbf{r}) \psi_e^\dagger(\mathbf{r}) \psi_\sigma(\mathbf{r}) + \text{h.c.} \right]. \quad (18)$$

The detuning frequency ω_{det} expresses the difference between the internal energy level difference and the frequency of the applied laser.

We calculate the “current” from the pairing state $|\sigma\rangle$, corresponding to the rate of the change in population of the e -state: $I(t) = \langle \dot{\mathcal{N}}_e(t) \rangle$. Here we divide the Hamiltonian in Eq. (15) into two parts: (i) The diagonal part $\tilde{\mathcal{H}}_0 = \mathcal{H}_{\text{MF}} + \mathcal{H}_e + \frac{\omega_{\text{det}}}{2} [\sum_\sigma \mathcal{N}_\sigma - \mathcal{N}_e]$ and (ii) the perturbation Hamiltonian \mathcal{H}_T . By following the linear response theory,⁸⁵ the tunneling current is given as

$$I^{(\sigma)}(t) = -i \int dt' \theta(t - t') \langle [\dot{\mathcal{N}}_e(t), \mathcal{H}_T^{(\sigma)}(t')] \rangle, \quad (19)$$

where the expression of the time-dependent quantity is given by $\mathcal{O}(t) = e^{i\tilde{H}_0 t} \mathcal{O} e^{-i\tilde{H}_0 t}$ with the canonical Hamiltonian $\tilde{H}_0 = \tilde{\mathcal{H}}_0 + \mu_e \mathcal{N}_e + \sum_\sigma \mu_\sigma \mathcal{N}_\sigma$. Especially, the tunneling Hamiltonian defined in Eq. (18) is transformed to

$$\mathcal{H}_T^{(\sigma)}(t) = \int d\mathbf{r} \Omega(\mathbf{r}) \left[e^{-i\tilde{\omega} t} \psi_e^\dagger(\mathbf{r}, t) \psi_\sigma(\mathbf{r}, t) + \text{h.c.} \right], \quad (20)$$

with the field operator in the Heisenberg representation, $\psi_e(\mathbf{r}, t) = e^{i\mathcal{H}_e t} \psi_e(\mathbf{r}) e^{-i\mathcal{H}_e t}$ and $\psi_\sigma(\mathbf{r}, t) = e^{i\mathcal{H}_{\text{MF}t}} \psi_\sigma(\mathbf{r}) e^{-i\mathcal{H}_{\text{MF}t}}$. Hereafter, we use the notation $\tilde{\omega} \equiv$

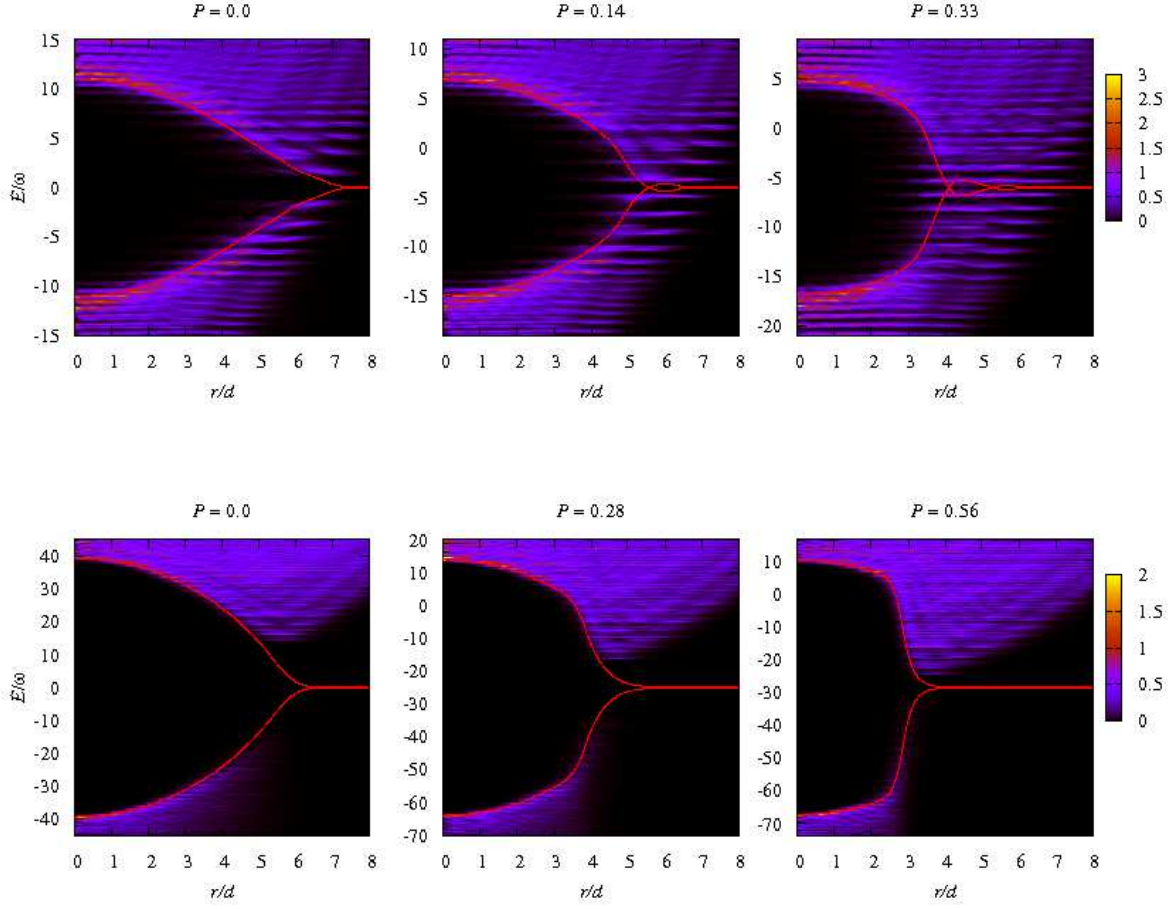


Fig. 10. (color online) Local density of states for majority species in various P 's: Top row is at the BCS side ($1/k_F a = -0.52$) and the bottom row is at the BEC side ($1/k_F a = +0.52$). The origin of the vertical axis corresponds to the energy equal to the chemical potential μ and the shift of the gap center from the origin is characterized by the mismatch $\delta\mu$. The solid lines denote the local energy gap defined by $\pm|\Delta(r)|$

$\omega_{\text{det}} + \mu_\sigma - \mu_e$ for convenience. Also, the number operator for the e -state obeys the Heisenberg equation, $i\dot{\mathcal{N}}_e(t) = [\mathcal{N}_e(t), \tilde{\mathcal{H}}]$, which leads to the following expression in the Heisenberg representation,

$$\dot{\mathcal{N}}_e(t) = -i \int d\mathbf{r} \Omega(\mathbf{r}) [e^{-i\tilde{\omega}t} \psi_e^\dagger(\mathbf{r}, t) \psi_\sigma(\mathbf{r}, t) - \text{h.c.}]. \quad (21)$$

By substituting Eqs (20) and (21) into the Kubo formula in Eq. (19), one can find that the total current is composed of two contributions, the single-particle tunneling current $I_S^{(\sigma)}$ and the Josephson tunneling current $I_J^{(\sigma)}$, as $I^{(\sigma)} \equiv I_S^{(\sigma)} + I_J^{(\sigma)}$. Since we are now interested in the single-particle tunneling, the Josephson current is neglected in the present situation. The resulting single-particle tunneling current is obtained from the analytic continuation of the quantity expressed as the product of Green's functions for the σ - and e -states:⁸⁵

$$I_S^{(\sigma)}(t) = 2\Im \int \int \mathcal{U}_\sigma(\mathbf{r}\mathbf{r}', i\omega_n \rightarrow \tilde{\omega} + i\eta) d\mathbf{r} d\mathbf{r}', \quad (22a)$$

where the Matsubara frequency is introduced as $\omega_n \equiv$

$\pi(2n+1)\beta$ and

$$\begin{aligned} \mathcal{U}_\uparrow(\mathbf{r}\mathbf{r}', i\omega_n) &= \beta^{-1} \Omega^*(\mathbf{r}) \Omega(\mathbf{r}') \sum_{\omega'_n} \\ &\times \mathcal{G}_{11}(\mathbf{r}'\mathbf{r}, i\omega'_n - i\omega_n) \mathcal{G}_e(\mathbf{r}\mathbf{r}', i\omega'_n), \end{aligned} \quad (22b)$$

$$\begin{aligned} \mathcal{U}_\downarrow(\mathbf{r}\mathbf{r}', i\omega_n) &= \beta^{-1} \Omega^*(\mathbf{r}) \Omega(\mathbf{r}') \sum_{\omega'_n} \\ &\times \mathcal{G}_{22}(\mathbf{r}'\mathbf{r}, i\omega'_n - i\omega_n) \mathcal{G}_e(\mathbf{r}\mathbf{r}', i\omega'_n). \end{aligned} \quad (22c)$$

The Green's function for the e -state is given as

$$\mathcal{G}_e(\mathbf{r}\mathbf{r}', i\omega_n) = \sum_{\zeta} \frac{\phi_\zeta(\mathbf{r}) \phi_\zeta^*(\mathbf{r}')}{i\omega_n - \epsilon_\zeta}, \quad (23)$$

where the eigenfunction and energy, ϕ_ζ and ϵ_ζ , are obtained from the Schrödinger equation for atoms in the e -state, $[H_e^{(0)} + \sum g_{e\sigma} \rho_\sigma] \phi_\zeta(\mathbf{r}) = \epsilon_\zeta \phi_\zeta(\mathbf{r})$. The expression of the Matsubara Green's function for the pairing state \mathcal{G}_{11} and \mathcal{G}_{22} are shown in Appendix B.

To this end, one can find the single-particle tunneling currents for the following distinguishable processes: For the tunneling from the majority species $|\sigma = \uparrow\rangle$ to the

e -state,

$$I_S^{(\uparrow)}(\tilde{\omega}) = 2\pi \sum_{\nu, \zeta} \left| \int \Omega(\mathbf{r}) u_\nu(\mathbf{r}) \phi_\zeta^*(\mathbf{r}) d\mathbf{r} \right|^2 \times [f_\nu - f(\epsilon_\zeta)] \delta(\tilde{\omega} + E_\nu - \epsilon_\zeta), \quad (24a)$$

and for the tunneling from the minority species $|\sigma = \downarrow\rangle$ to the e -state,

$$I_S^{(\downarrow)}(\tilde{\omega}) = 2\pi \sum_{\nu, \zeta} \left| \int \Omega(\mathbf{r}) v_\nu^*(\mathbf{r}) \phi_\zeta^*(\mathbf{r}) d\mathbf{r} \right|^2 \times [f_\nu - f(\epsilon_\zeta)] \delta(\tilde{\omega} - E_\nu - \epsilon_\zeta). \quad (24b)$$

Note that in the same sense as the BdG formalism in Sec. 2, the sum in above Eqs. (24a) and (24b) is done for all eigenstates both positive and negative energies because of the breaking of the time-reversal symmetry.

In performing the numerical calculation, the δ -function in Eq. (24) is replaced to the Lorentzian function $\delta(z) \rightarrow \Gamma_\eta(z) = (\eta/2)^2 / [z^2 + (\eta/2)^2]$, where the resolution of the spectrum η is set as $\eta = 1.0\omega$ throughout this paper. Also, we consider the following situations: (i) The interaction between the pairing state and the e -state is negligible, $g_{e\sigma} = 0$. (ii) We focus on the transition from the pairing state $|\sigma\rangle$ to the excited state $|e\rangle$, i.e., the positive detuning $\omega_{\text{det}} > 0$ and $I_S^{(\sigma)} > 0$.

4.3 Numerical results

It is important to mention that the tunneling current in the homogeneous pairing field $\Delta(\mathbf{r}) = \Delta$ at $P = 0$ is expressed as

$$I_S^{(\sigma)}(\omega_{\text{det}}) = - \sum_{\mathbf{p}, \mathbf{q}} |\Omega_{\mathbf{p}\mathbf{q}}|^2 \int_{-\infty}^{\infty} \frac{d\xi}{2\pi} [f(\xi - \mu_e + \omega_{\text{det}}) - f(\xi - \mu_e)] \mathcal{N}_\sigma(\mathbf{q}, \xi - \mu_\sigma) \mathcal{N}_e(\mathbf{p}, \xi + \omega_{\text{det}} - \mu_e), \quad (25)$$

with $\Omega_{\mathbf{p}\mathbf{q}} \equiv \int d\mathbf{r} e^{i\mathbf{p}\cdot\mathbf{r}} \Omega(\mathbf{r}) e^{-i\mathbf{q}\cdot\mathbf{r}}$. The density of states for the pairing state,

$$\mathcal{N}_\sigma(\mathbf{q}, z) = 2\pi [u_{\mathbf{q}}^2 \delta(z - E_{\mathbf{q}}) + v_{\mathbf{q}}^2 \delta(z + E_{\mathbf{q}})], \quad (26)$$

and for the e -state, $\mathcal{N}_e(z) = 2\pi \delta(z - \epsilon_{\mathbf{p}})$. Here, $(u_{\mathbf{q}}, v_{\mathbf{q}})$ and $E_{\mathbf{q}}$ are the solution of the BdG equation in the homogeneous system at $P = 0$, and $\epsilon_{\mathbf{p}} = p^2/2m - \mu_e$ is the eigenenergy of a free particle in the e -state. We are now interested in the situation with the positive detuning and current, $\omega_{\text{det}} > 0$ and $I_S^{(\sigma)} > 0$, which expresses the fraction loss of the pairing σ -state. First, one finds the following simple result in the case of $\Delta = 0$,

$$I_S^{(\sigma)}(\omega_{\text{det}}) = 2\pi \Omega^2 (N_\sigma - N_e) \delta(\omega_{\text{det}}), \quad (27)$$

which leads to the single peak structure at $\omega_{\text{det}} = 0$ when the e -state is initially not occupied ($\mu_e = 0$). The intensity of the peak gradually becomes small with increasing μ_e and in the case of the equal chemical potential $\mu_e = \mu_\sigma$ the tunneling current is not responsible, i.e., $I_S^{(\sigma)} = 0$.

For the pairing state $\Delta \neq 0$, after evaluating the integral over energy and momenta in Eq. (25), one find⁸⁰

$$I_S^{(\sigma)}(\omega_{\text{det}}) = \pi \Omega^2 \mathcal{N}_0 \left(\frac{\omega_{\text{det}}^2 - \Delta^2}{\omega_{\text{det}}} + 2\mu_\sigma \right) \frac{\Delta^2}{\omega_{\text{det}}^2}$$

$$\times \Theta(\omega_{\text{det}}^2 - \Delta^2 + 2\delta\tilde{\mu}\omega_{\text{det}}), \quad (28)$$

where we introduce the density of states in the ideal Fermi gas, $\mathcal{N}_0(E) = \frac{V}{2\pi^2} \sqrt{E}$. Also, we set $\delta\tilde{\mu} \equiv \mu_\sigma - \mu_e$. For the positive detuning $\omega_{\text{det}} > 0$ and the system with the positive chemical potential $\mu_\sigma > 0$, it is found the the function $I_S^{(\sigma)}(\omega_{\text{det}})$ becomes the monotonic decrease function with the range $\omega_{\text{det}}/E_F > \Delta/E_F$, when the e -state is initially occupied, $\mu_e = \mu_\sigma$. In contrast, in the case of $\mu_e = 0$, the resonant detuning at which $I_S^{(\sigma)}$ has the maximum value is shifted to $\omega_{\text{det}}/E_F = \frac{5}{8}(\frac{\Delta}{E_F})^2$. In the deep BEC limit where $\mu_\sigma < 0$ and $\Delta/|\mu_\sigma| \ll 1$, $I_S^{(\sigma)}$ exhibits the different behavior from that in the BCS side, which is insensitive to μ_e . Then, the resonant detuning is situated around $\omega_{\text{det}}/E_F \sim 2|\mu_\sigma|/E_F \sim |E_b|/E_F$. This energy corresponds to the dissociation of molecular bosons and is uniquely characterized by the dimensionless parameter $1/(k_F a)^2$.

In Fig. 11, we display the numerical results on the fraction loss of the minority species $I_S^{(\downarrow)}$ in the imbalanced systems in the presence of the harmonic trap where (a) and (b) correspond to the BCS and BEC sides, respectively. Hereafter, we consider the situation that the e -state is initially empty, $\mu_e = 0$. Also, we set $\Omega(\mathbf{r}) = \Omega$. In the BCS side, as shown in Fig. 11(a), the resonant detuning in low P 's is situated around $\omega_{\text{det}}/E_F \simeq 0.1$, which is related to the dissociate energy of the fermionic

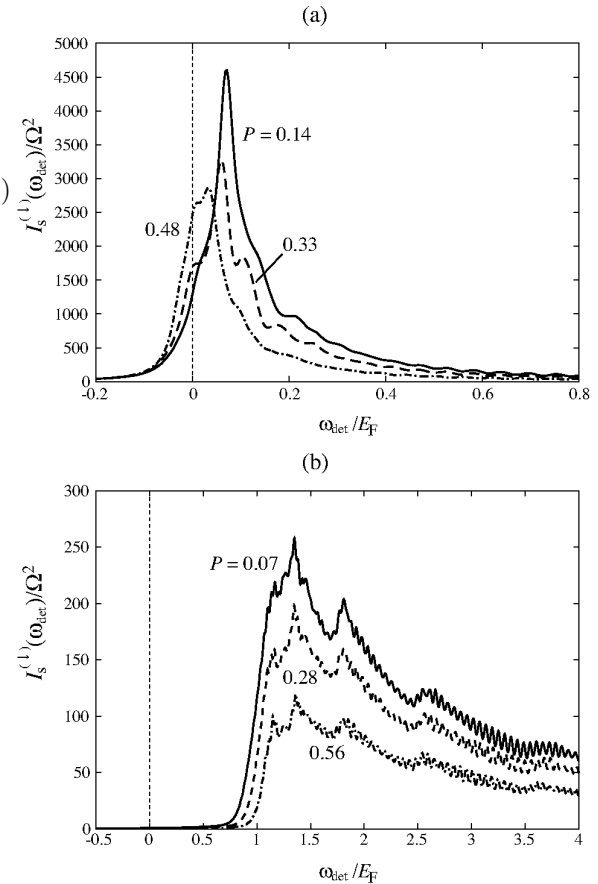


Fig. 11. The RF spectroscopy of the minority component $I_S^{(\downarrow)}$ at $1/k_F a = -0.52$ (a) and 0.52 (b) with $N = 3,000$ atoms. All the results are at $T = 0$.

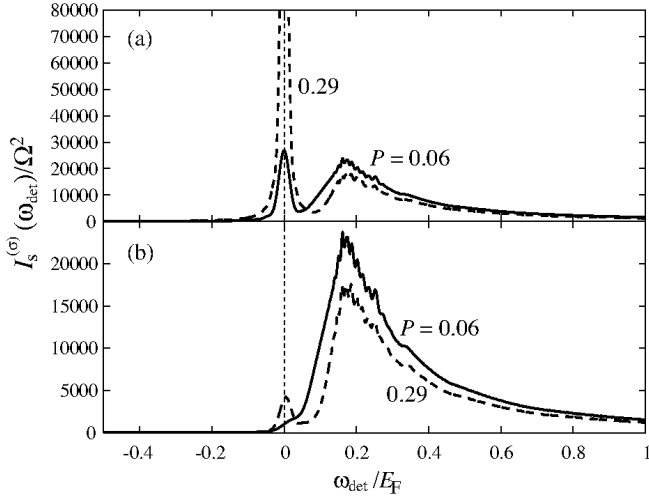


Fig. 12. The fraction loss of the majority (a) and minority species (b) at $1/k_F a = -0.14$ with $N = 150,000$ atoms. All the results are at $T = 0$.

pairing described above, $\omega_{\text{det}}/E_F \sim (\Delta_0/E_F)^2$, with the maximum gap $\Delta_0 = 0.34E_F = 11\omega$. As P increases, the peak position approaches the zero detuning. We should notice that in high P 's, the fraction loss additionally occurs at the zero detuning and the resulting spectrum profile yields the double peak structure. This reveals the fact that the system under the high imbalance is in the pairing state with the partially polarized spins, which is indirect evidence of the FFLO state. As seen in Fig. 10, the mid-gap state appears in the spacing between the small energy gap near the surface ($r/d \sim 6$) when $P \neq 0$. The presence of the mid-gap state increases the intensity of the fraction loss at $\omega_{\text{det}} = 0$.

It is seen from Fig. 11(b) that the fraction loss in the BEC side yields the distinctive spectrum from that in the BCS side. There are two differences: (i) The detuning at which the fermionic/molecular pairs are dissociated is unchanged against the increase of P 's. Only the intensity becomes weak. (ii) With increasing P , no additional peak appears around the zero detuning. This is because all the minority spins in the imbalanced situation forms the “pair” with the corresponding amount of the majority species in the local, and the spins in the normal state are fully polarized. We should mention that the fraction loss for the majority species are unchanged in the extensive region from the BCS to BEC limit, where the spectrum always yields the double peak structure whose one peak is situated with large intensity at $\omega_{\text{det}} = 0$ and another depends on the dissociation energy of fermionic or molecular pairs at $\omega_{\text{det}} \simeq \Delta_0$.

Finally, the RF spectroscopy for the system with a realistic number $N = 150,000$ in the vicinity of the unitary limit $1/k_F a = -0.14$ is presented in Fig. 12. The qualitative behavior is unchanged from the case of the small particle number displayed in Fig. 11, that is, the fraction loss of the minority species occurs at the zero detuning in addition to $\omega_{\text{det}}/E_F \sim \frac{5}{8}(\frac{\Delta_0}{E_F})^2 = 0.17$ corresponding to the dissociation energy of the pairing state at $r = 0$, $\Delta_0 = 0.53E_F = 82\omega$. The corresponding pairing field is

shown in Fig. 8 where the FFLO modulation appears in the vicinity of the boundary between the equal pairing core and polarized normal domain. It should be emphasized that the satellite peak at the zero detuning is the indirect evidence for the FFLO pairing. This prediction can be experimentally checked by carefully examining the RF spectroscopy in the lower temperature region.⁸ Also note that this spectrum presented in Fig. 12 is in good agreement with that obtained from the non-linear response theory.⁵²

5. Concluding remarks

In this paper, we have theoretically studied the stable superfluid state in strongly interacting trapped Fermi systems with population imbalance, based on the single-channel Hamiltonian. We numerically solve the Bogoliubov-de Gennes equation coupled with the regularized gap equation and number equation in the BCS-BEC crossover under imbalanced spin densities, where the computation for the higher energy contribution is supplemented by the local density approximation.

The main results are divided into two: (1) First, in Sec. 3, we have discussed the ground state in the crossover regime under population imbalance and have presented the quantum phase diagram in a $1/k_F a$ - P plane. In the weak coupling regime ($1/k_F a < 0$), it has been found that the resulting pairing field at $T = 0$ exhibits the FFLO oscillation around the edge of the minority component. In particular, the pairing field exhibits the oscillation in the entire region of the system when P approaches P_c . This novel pairing state is reflected in the density and local “magnetization” profiles, such as the bimodal structure in the minority species. In contrast, the FFLO oscillation disappears in the whole P 's of the BEC regime, where the resulting ground state yields the phase separation between the balanced pairing domain and fully polarized spin domain. We have found that the spatial variation of the pairing field affects the density: For instance, the presence of the FFLO modulated pairing field leads to the partially polarized spin density, while the PS state is reflected in the fully polarized spins. It has also been shown that the FFLO modulation survives even in the unitary limit, as the proximity effect. We have confirmed that these tendencies on the ground state structure are unchanged in the system with the realistic particle number $N \sim \mathcal{O}(10^5)$, which is comparable with the recent experiments.³⁻⁸ Our calculation reproduce the PS-like profile in the local magnetization, while the pairing field yields the FFLO modulation even in the vicinity of the resonance. The periodicity and intensity of the modulation increase as $1/k_F a$ approaches the weak coupling BCS regime. In particular, we have found that the periodicity L of the FFLO oscillation is well scaled with the coherence length ξ_0 as $L \sim 3\xi_0$, throughout the extensive range on $k_F a \leq 0$ and $P < P_c$.

(2) The second part of the present paper has been devoted to the another observable quantity, the radio-frequency spectroscopy. By numerically solving the “tunneling current” derived from the linear response theory, the contributions of the pairing field to the spectrum have been discussed. The clear difference of the resonant

shape between the BCS and BEC sides reveals the different superfluid state, which can be checked in the further experimental efforts.

Note that in the phase contrast imaging of the local “magnetization” by the MIT experiment,⁷ the PS-like profile was observed at the unitary limit $1/k_F a = 0$. The our results presented in Figs. 6 and 8 are in good agreement with it, which predicts that the “pairing field” exhibits the FFLO oscillation in the edge of the cloud. Also, we have demonstrated that as the system approaches the weak coupling BCS regime, the FFLO modulation covers the entire region of the system especially at $P \sim P_c$. The previous experiment⁵ has already observed the quantum phase transition in the BCS side of a resonance, $1/k_F a \sim -0.4$, which is the favorable situation for the detection of the FFLO. The further detailed analysis may catch the signature of the FFLO pairing via the density and the RF spectroscopy as we has described in the present paper.

Finally, we mention the thermodynamic stability of the FFLO phase against the increase of T . In Fig. 13, we present the phase diagram in a T - P plane at a BCS side. The resulting phase diagram yields the multiple superfluid phases composed of the FFLO and the non-oscillating BCS states. All three phase transition lines in between the BCS, FFLO, and normal states are of the second order and these lines meet at the so-called Lifshitz (L) point.⁸⁶ The BCS-FFLO line starts right from $P = T = 0$, implying that the ground state is always FFLO when $P \neq 0$ and low T 's. The BCS appears only at the higher T 's. This second-phase transition via the FFLO state may be realized in the weak coupling regime, while in the strong coupling regime the first-order transition is predicted by the LDA calculation⁴⁴ in which the Lifshitz point is replaced to the tricritical point. We also note that this L point exhibits the universal temperature $T_L/T_{c0} \simeq 0.6$ in the weak coupling regime, independent from the coupling constant $1/k_F a$. Hence, all three second order lines are uniquely determined with a fixed L point. The similar phase diagram has been proposed even in the absence of the trap potential.²⁹

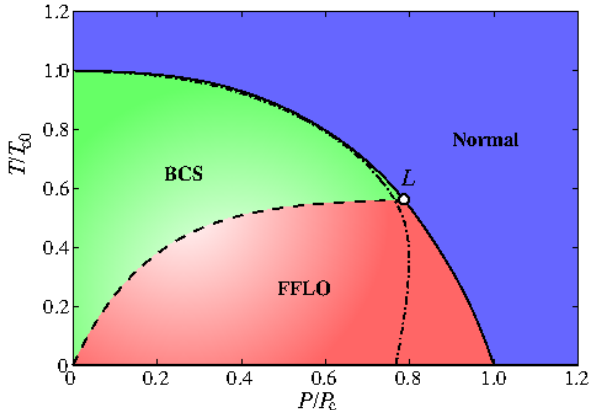


Fig. 13. (color online) Typical T - P phase diagram in the weak coupling BCS side of a resonance ($1/k_F a = -0.75$). The dashed-dotted line denotes T_c for the non-oscillating BCS state.⁴⁹ Empty circle is the Lifshitz point.

One of the main outcomes in the current work is that the FFLO modulated pairing field survives in the whole region in the system approaching the weak coupling limit ($1/k_F a \rightarrow -\infty$). The calculation presented here has been performed in the system restricted in the cylindrical geometry. The FFLO oscillating pattern in the fully three-dimensional system without any restriction, such as a elongated cigar-shaped or disk-shaped trap, is yet open to question, which should be explored further in future.

Acknowledgements

The authors acknowledge support by the Grant-in-Aid for Scientific Research, Japan Society for the Promotion of Science.

Appendix A: Regularized BdG equation

We start with the original Hamiltonian, in Eq. (2). Here, it is convenient to introduce a spinor in the Nambu space,

$$\Psi(\mathbf{r}) = [\psi_\uparrow(\mathbf{r}), \psi_\downarrow^\dagger(\mathbf{r})]^T. \quad (\text{A.1})$$

Applying the standard mean-field approximation to the interaction part of the above Hamiltonian, Eq. (2), the effective Hamiltonian can be derived as

$$\mathcal{H}_{\text{MF}} = \mathcal{E}_0 + \int d\mathbf{r} \int d\mathbf{r}' \Psi^\dagger(\mathbf{r}) \hat{\mathcal{K}}(\mathbf{r}, \mathbf{r}') \Psi(\mathbf{r}'), \quad (\text{A.2})$$

where

$$\hat{\mathcal{K}}(\mathbf{r}, \mathbf{r}') \equiv \begin{bmatrix} \mathcal{K}_\uparrow(\mathbf{r}, \mathbf{r}') & \Delta(\mathbf{r}, \mathbf{r}') \\ \Delta^*(\mathbf{r}, \mathbf{r}') & -\mathcal{K}_\downarrow(\mathbf{r}, \mathbf{r}') \end{bmatrix}, \quad (\text{A.3a})$$

$$\mathcal{K}_\sigma(\mathbf{r}, \mathbf{r}') = H_\sigma^{(0)} \delta(\mathbf{r} - \mathbf{r}') + \mathcal{W}_\sigma(\mathbf{r}, \mathbf{r}'). \quad (\text{A.3b})$$

The mean-field quantities, the pairing potential $\Delta(\mathbf{r}, \mathbf{r}')$ and the Hartree potential $\mathcal{W}_\sigma(\mathbf{r}, \mathbf{r}')$, are defined by

$$\Delta(\mathbf{r}, \mathbf{r}') \equiv U(\tilde{r}) \langle \psi_\downarrow(\mathbf{r}') \psi_\uparrow(\mathbf{r}) \rangle, \quad (\text{A.4a})$$

$$\mathcal{W}_\sigma(\mathbf{r}, \mathbf{r}') \equiv U(\tilde{r}) \rho_\sigma(\mathbf{r}) = U(\tilde{r}) \langle \psi_\sigma^\dagger(\mathbf{r}) \psi_\sigma(\mathbf{r}') \rangle. \quad (\text{A.4b})$$

\mathcal{E}_0 is the c -number including the condensation and Hartree energies and $\tilde{r} \equiv |\tilde{\mathbf{r}}| = \mathbf{r} - \mathbf{r}'$ is the relative coordinate.

The Bogoliubov transformation of the spinor $\Psi(\mathbf{r})$ into the quasiparticle basis $\eta_\nu \equiv [\eta_{\nu,\uparrow}, \eta_{\nu,\downarrow}^\dagger]^T$ is defined by

$$\Psi(\mathbf{r}) = \sum_\nu \begin{bmatrix} u_\nu(\mathbf{r}) & -v_\nu^*(\mathbf{r}) \\ v_\nu(\mathbf{r}) & u_\nu^*(\mathbf{r}) \end{bmatrix} \eta_\nu \equiv \sum_\nu \hat{u}_\nu(\mathbf{r}) \eta_\nu. \quad (\text{A.5})$$

Here the creation and annihilation operators of the quasiparticles, $\eta_{\nu,\sigma}^\dagger$ and $\eta_{\nu,\sigma}$, obey the fermionic commutation relations. The quasiparticle wave function in the matrix form $\hat{u}_\nu(\mathbf{r})$ satisfies the orthonormal condition,

$$\int d\mathbf{r} \hat{u}_\nu^\dagger(\mathbf{r}) \hat{u}_{\nu'}(\mathbf{r}) = \delta_{\nu,\nu'}. \quad (\text{A.6})$$

Also, we use the completeness in a matrix form,

$$\sum_\nu \hat{u}_\nu(\mathbf{r}) \hat{u}_\nu^\dagger(\mathbf{r}') = \delta(\mathbf{r} - \mathbf{r}'). \quad (\text{A.7})$$

Then, we assume that the mean-field Hamiltonian can be transformed into the diagonalized form, $\mathcal{H}_{\text{MF}} = \mathcal{E}_0 + \sum_\nu \sum_\sigma \varepsilon_\nu^{(\sigma)} \eta_{\nu,\sigma}^\dagger \eta_{\nu,\sigma}$. To this end, we obtain the

Bogoliubov-de Gennes equation,

$$\int d\mathbf{r}' \hat{\mathcal{K}}(\mathbf{r}, \mathbf{r}') \hat{u}_\nu(\mathbf{r}') = \hat{u}_\nu(\mathbf{r}) \begin{bmatrix} \varepsilon_\nu^{(\uparrow)} & \\ & -\varepsilon_\nu^{(\downarrow)} \end{bmatrix}. \quad (\text{A}\cdot 8)$$

The above BdG matrix $\hat{\mathcal{K}}$ yields the double eigenstates for hyperfine spins; To see this, we set the eigenfunction with the up-spin as $\varphi_\nu^{(\uparrow)} \equiv [u_\nu, v_\nu]^T$, having the eigenvalue $\varepsilon_\nu^{(\uparrow)}$: $\hat{\mathcal{K}}\varphi_\nu^{(\uparrow)} = \varepsilon_\nu^{(\uparrow)}\varphi_\nu^{(\uparrow)}$. It is found that the BdG equation (A-8) simultaneously has the eigenstates for down-spins $\varphi_\nu^{(\downarrow)} \equiv [-v_\nu^*, u_\nu^*]^T$ with the eigenvalue $-\varepsilon_\nu^{(\downarrow)}$. Therefore, once one solves the BdG equation

$$\int d\mathbf{r}' \hat{\mathcal{K}}(\mathbf{r}, \mathbf{r}') \varphi_\nu(\mathbf{r}') = E_\nu \varphi_\nu(\mathbf{r}), \quad (\text{A}\cdot 9)$$

with the eigenfunction $\varphi_\nu \equiv [u_\nu, v_\nu]^T$ and the eigenstates E_ν corresponding to both ones for up- and down-spins. However, we should emphasize that $\varepsilon_\nu^{(\uparrow)} \neq \varepsilon_\nu^{(\downarrow)}$ because the finite mismatch of the Fermi surface causes the breaking of the time-reversal symmetry, $\hat{\mathcal{K}}(\mathbf{r}, \mathbf{r}') \neq -\hat{\tau}_2 \hat{\mathcal{K}}^*(\mathbf{r}, \mathbf{r}') \hat{\tau}_2$, where $\hat{\tau}_j$ is the j -th Pauli matrix.

With the eigenstates in Eq. (A-9), the pairing field defined in Eq. (A-4a) can be explicitly expressed as

$$\begin{aligned} \Delta(\mathbf{r}, \mathbf{r}') &= U(\tilde{r}) \sum_\nu \left[u_\nu(\mathbf{r}) v_\nu^*(\mathbf{r}') f_\nu^{(\uparrow)} - v_\nu^*(\mathbf{r}) u_\nu(\mathbf{r}') f_\nu^{(\downarrow)} \right] \\ &= U(\tilde{r}) \sum_\nu u_\nu(\mathbf{r}) v_\nu^*(\mathbf{r}') f_\nu, \end{aligned} \quad (\text{A}\cdot 10)$$

where the Fermi distribution function $f_\nu^{(\uparrow)} \equiv f(\varepsilon_\nu^{(\uparrow)}) = \langle \eta_{\nu', \uparrow}^\dagger \eta_{\nu, \uparrow} \rangle \delta_{\nu, \nu'}$, $f_\nu^{(\downarrow)} \equiv f(-\varepsilon_\nu^{(\downarrow)}) = \langle \eta_{\nu', \downarrow}^\dagger \eta_{\nu, \downarrow} \rangle \delta_{\nu, \nu'}$, and $f_\nu \equiv f(E_\nu) = 1/(e^{E_\nu/T} + 1)$. The sum in the final expression of the gap equation (A-10) is done for all the eigenstates with both positive and negative eigenenergies. Then, the particle density in each spin state is given from Eqs. (A-4b) and (A-5), which is described in Eq. (9). The BdG equation (A-9) is now self-consistently solved with the mean-field conditions, Eqs. (A-10) and (9), for the fixed total particle number: $N = \sum_\sigma N_\sigma = \int d\mathbf{r} \sum_\sigma \rho_\sigma(\mathbf{r})$.

Now, let us spell out the explicit expression in the equal mixture of two-component fermions, i.e., $\mathcal{K}_\uparrow = \mathcal{K}_\downarrow$ under $\delta\mu = 0$. Then, the BdG matrix (A-3a) yields the time-reversal symmetry, $\hat{\mathcal{K}}(\mathbf{r}, \mathbf{r}') = -\hat{\tau}_2 \hat{\mathcal{K}}^*(\mathbf{r}, \mathbf{r}') \hat{\tau}_2$. It hence follows that a positive eigenvalue E_ν having the eigenfunction $\varphi_\nu \equiv [u_\nu, v_\nu]^T$ in Eq. (A-9) is always accompanied by the negative eigenvalue $-E_\nu$ with the eigenfunction $-i\hat{\tau}_2 \varphi_\nu^* \equiv [-v_\nu^*, u_\nu^*]^T$. Then, the mean-field quantities shown in Eqs. (A-10) and (9) can be reduced to the standard form,

$$\Delta(\mathbf{r}, \mathbf{r}') = U(\tilde{r}) \sum_{E_\nu \geq 0} u_\nu(\mathbf{r}) v_\nu^*(\mathbf{r}') [2f_\nu - 1], \quad (\text{A}\cdot 11a)$$

$$\rho_\sigma(\mathbf{r}) = \sum_{E_\nu \geq 0} [|u_\nu(\mathbf{r})|^2 f_\nu + |v_\nu(\mathbf{r})|^2 (1 - f_\nu)]. \quad (\text{A}\cdot 11b)$$

Hereafter, we use the definition in the case of the system without the time-reversal symmetry.

At low temperatures, the collisions between atoms can be described within the s -wave scattering, $U(\tilde{r}) = g\delta(\tilde{\mathbf{r}})$.

Here, $g = 4\pi^2 a/M$ is the coupling constant and in general the interaction can be expressed with the dimensionless parameter $k_F a$ where $k_F \equiv \sqrt{2ME_F}$ is the Fermi wave vector of non-interacting Fermi gas estimated with the Fermi energy E_F . Then, the BdG equation (A-9) is reduced to the following local form:

$$\begin{bmatrix} \mathcal{K}_\uparrow(\mathbf{r}) & \Delta(\mathbf{r}) \\ \Delta^*(\mathbf{r}) & -\mathcal{K}_\downarrow^*(\mathbf{r}) \end{bmatrix} \begin{bmatrix} u_\nu(\mathbf{r}) \\ v_\nu(\mathbf{r}) \end{bmatrix} = E_\nu \begin{bmatrix} u_\nu(\mathbf{r}) \\ v_\nu(\mathbf{r}) \end{bmatrix} \quad (\text{A}\cdot 12)$$

where $\Delta(\mathbf{r}, \mathbf{r}') = \delta(\tilde{\mathbf{r}}) \Delta(\mathbf{r})$ and $\mathcal{K}_\sigma(\mathbf{r}, \mathbf{r}') = \delta(\tilde{\mathbf{r}}) \mathcal{K}_\sigma(\mathbf{r})$.

Here, there are two singular contributions to the BdG equation (A-12) and gap equation (A-10). First, the Hartree potential $g\rho_\sigma$ diverges at the unitary limit, which is neglected throughout this paper (see the text in Sec. II A, for details). The second singular behavior arises the fact that the contact interaction leads to an ultra-violet (UV) divergence of a pairing field defined in Eq. (A-10), where the leading term of $\Delta(\mathbf{r}, \mathbf{r}')$ behaves as $-M\Delta(\mathbf{r})/4\pi\tilde{r}$ at $\tilde{r} \rightarrow 0$:

$$\Delta(\mathbf{r}, \mathbf{r}') = -\frac{M}{4\pi\tilde{r}} \Delta(\mathbf{R}) + g\mathcal{F}_{\text{reg}}(\mathbf{R}, \tilde{\mathbf{r}}) + \mathcal{O}(\tilde{\mathbf{r}}), \quad (\text{A}\cdot 13)$$

where \mathcal{F}_{reg} is the regular part of the anomalous average $\mathcal{F}(\mathbf{R}, \tilde{\mathbf{r}}) = \langle \psi_\downarrow(\mathbf{r}') \psi_\uparrow(\mathbf{r}) \rangle$ ($\mathbf{R} \equiv (\mathbf{r} + \mathbf{r}')/2$ is the center-of-mass coordinate). One way to remove the divergent term is to replace the original contact interaction g to the pseudo-potential^{56–59} and then, the formal expression of the pairing field is given by

$$\Delta(\mathbf{r}) = g \lim_{\tilde{\mathbf{r}} \rightarrow 0} \frac{\partial}{\partial \tilde{\mathbf{r}}} [\tilde{r} \langle \psi_\downarrow(\mathbf{r}') \psi_\uparrow(\mathbf{r}) \rangle]. \quad (\text{A}\cdot 14)$$

To give the straightforward expression of the regularization operator $\lim_{\tilde{\mathbf{r}} \rightarrow 0} \partial_{\tilde{\mathbf{r}}}[\cdot]$, we introduce the single-particle Green's function, $G_\mu(\mathbf{r}, \mathbf{r}') = \langle \mathbf{r} | H_0^{-1} | \mathbf{r}' \rangle$ with $\delta\mu = 0$. This function yields the same nature of divergence with Δ in the limit of $\tilde{r} \rightarrow 0$: $G_\mu(\mathbf{R}, \tilde{\mathbf{r}}) = \frac{M}{2\pi\tilde{r}} + G_\mu^{\text{reg}}(\mathbf{R}) + \mathcal{O}(\tilde{\mathbf{r}})$. Here, the divergent contribution of the anomalous average can be canceled out by the irregular part of the single-Green's function in the second term of the right-hand side, which allows one to introduce an explicit energy cutoff. By employing the local density approximation, finally we obtain the regularized gap equation,^{58, 59}

$$\Delta(\mathbf{r}) = \tilde{g}(\mathbf{r}) \sum_\nu u_\nu(\mathbf{r}) v_\nu^*(\mathbf{r}) f_\nu, \quad (\text{A}\cdot 15)$$

where the renormalized coupling constant $\tilde{g}(\mathbf{r})$,

$$\frac{1}{\tilde{g}(\mathbf{r})} = \frac{1}{g} + \frac{Mk_c(\mathbf{r})}{2\pi^2} \left[1 - \frac{k_F(\mathbf{r})}{2k_c(\mathbf{r})} \ln \frac{k_c(\mathbf{r}) + k_F(\mathbf{r})}{k_c(\mathbf{r}) - k_F(\mathbf{r})} \right] \quad (\text{A}\cdot 16)$$

Here, $k_F(\mathbf{r})$ and $k_c(\mathbf{r})$ are the local wave vectors defined by the local Fermi and cutoff energies, respectively (see Eq. (7)).

Appendix B: Matsubara Green's functions

The Matsubara Green's function in the Nambu space is defined with the imaginary time τ as

$$\hat{\mathcal{G}}(1, 2) = -\left\langle T_\tau \left[\Psi(1) \Psi^\dagger(2) \right] \right\rangle. \quad (\text{B}\cdot 1)$$

Here we introduce the notation $1 \equiv (\mathbf{r}_1, \tau_1)$. The Green's function in a 2×2 matrix form obeys the Gor'kov equation

tion⁸⁷

$$\int d2 \left[-\frac{\partial}{\partial \tau} \hat{\tau}_0 \delta(1, 2) - \hat{\mathcal{K}}(1, 2) \right] \hat{\mathcal{G}}(2, 1') = \hat{\tau}_0 \delta(1, 1'), \quad (\text{B-2})$$

with a 2×2 unit matrix $\hat{\tau}_0$. Also, we set $\hat{\mathcal{K}}(1, 2) \equiv \delta(\tau_1 - \tau_2) \hat{\mathcal{K}}(\mathbf{r}_1, \mathbf{r}_2)$. From the BdG equation (A-8), $\hat{\mathcal{K}}(\mathbf{r}_1, \mathbf{r}_2)$ may be expanded as

$$\hat{\mathcal{K}}(\mathbf{r}_1, \mathbf{r}_2) = \sum_{\nu} \hat{u}_{\nu}(\mathbf{r}_1) \begin{bmatrix} \varepsilon_{\nu}^{(\uparrow)} & \\ & -\varepsilon_{\nu}^{(\downarrow)} \end{bmatrix} \hat{u}_{\nu}^{\dagger}(\mathbf{r}_2). \quad (\text{B-3})$$

The Green's function becomes diagonal in the representation where $\hat{\mathcal{K}}$ is. Hence, $\hat{\mathcal{G}}(1, 2)$ may be expanded as

$$\hat{\mathcal{G}}(1, 2) = \frac{1}{\beta} \sum_n e^{-i\omega_n(\tau_1 - \tau_2)} \sum_{\nu} \hat{u}_{\nu}(\mathbf{r}_1) \hat{\mathcal{G}}_{\nu}(i\omega_n) \hat{u}_{\nu}^{\dagger}(\mathbf{r}_2). \quad (\text{B-4})$$

Its Fourier component $\hat{\mathcal{G}}^{<(0)}(\varepsilon)$ is obtained easily as

$$\hat{\mathcal{G}}_{\nu}(i\omega_n) = \begin{bmatrix} (i\omega_n - \varepsilon_{\nu}^{(\uparrow)})^{-1} & 0 \\ 0 & (i\omega_n + \varepsilon_{\nu}^{(\downarrow)})^{-1} \end{bmatrix}. \quad (\text{B-5})$$

It is convenient to introduce the Fourier transform with respect to τ , $\hat{\mathcal{G}}(1, 2) = \beta^{-1} \sum_n e^{-i\omega_n(\tau_1 - \tau_2)} \hat{\mathcal{G}}(\mathbf{r}_1, \mathbf{r}_2, i\omega_n)$, whose coefficient is obtained from Eq. (B-4). With the eigenfunctions and energy of the BdG equation, (u_{ν}, v_{ν}) and E_{ν} , the expression of $\hat{\mathcal{G}}(\mathbf{r}_1, \mathbf{r}_2, i\omega_n)$ is given by

$$\mathcal{G}_{11}(\mathbf{r}_1, \mathbf{r}_2, i\omega_n) = \sum_{\nu} \frac{u_{\nu}(\mathbf{r}_1) u_{\nu}^*(\mathbf{r}_2)}{i\omega_n - E_{\nu}}, \quad (\text{B-6a})$$

$$\mathcal{G}_{12}(\mathbf{r}_1, \mathbf{r}_2, i\omega_n) = \sum_{\nu} \frac{u_{\nu}(\mathbf{r}_1) v_{\nu}^*(\mathbf{r}_2)}{i\omega_n - E_{\nu}}, \quad (\text{B-6b})$$

$$\mathcal{G}_{21}(\mathbf{r}_1, \mathbf{r}_2, i\omega_n) = \sum_{\nu} \frac{v_{\nu}(\mathbf{r}_1) u_{\nu}^*(\mathbf{r}_2)}{i\omega_n - E_{\nu}}, \quad (\text{B-6c})$$

$$\mathcal{G}_{22}(\mathbf{r}_1, \mathbf{r}_2, i\omega_n) = \sum_{\nu} \frac{v_{\nu}(\mathbf{r}_1) v_{\nu}^*(\mathbf{r}_2)}{i\omega_n - E_{\nu}}, \quad (\text{B-6d})$$

where \mathcal{G}_{ij} denotes the (i, j) element of the 2×2 matrix $\hat{\mathcal{G}}$.

- 1) D.E. Sheehy and L. Radzihovsky: Ann. Phys. in press (cond-mat/0607803).
- 2) See, for example, R. Casalbuoni and G. Nardulli: Rev. Mod. Phys. **76** (2004) 263.
- 3) G.B. Partridge, W. Li, R.I. Kamar, Y. Liao, and R. Hulet: Science **311** (2006) 503.
- 4) G.B. Partridge, W. Li, Y.A. Liao, R.G. Hulet, M. Haque, H.T.C. Stoof: Phys. Rev. Lett. **97** (2006) 190407.
- 5) M.W. Zwierlein, A. Schirotzek, C.H. Schunck, and W. Ketterle: Science **311** (2006) 492.
- 6) M.W. Zwierlein, C.H. Schunck, A. Schirotzek, W. Ketterle: Nature **442** (2006) 54.
- 7) Y. Shin, M.W. Zwierlein, C.H. Schunck, A. Schirotzek, W. Ketterle: Phys. Rev. Lett. **97** (2006) 030401.
- 8) C.H. Schunck, Y. Shin, A. Schirotzek, M.W. Zwierlein, W. Ketterle: cond-mat/0702066.
- 9) See for review, Q. Chen, J. Stajic, S. N. Tan, and K. Levin:

Phys. Rep. **412** (2005) 1.

- 10) A.M. Clogston: Phys. Rev. Lett. **9** (1962) 266.
- 11) P. Fulde and R.A. Ferrell: Phys. Rev. **135** (1964) A550.
- 12) A.I. Larkin and Y.N. Ovchinnikov: Sov. Phys. JETP **20** (1965) 762.
- 13) P.F. Bedaque, H. Caldas, and G. Rupak: Phys. Rev. Lett. **91** (2003) 247002.
- 14) W.V. Liu and F. Wilczek: Phys. Rev. Lett. **90** (2003) 047002.
- 15) H. Muther and A. Sedrakian: Phys. Rev. Lett. **88** (2002) 252503.
- 16) A. Sedrakian, J. Mur-Petit, A. Polls, and H. Muther: Phys. Rev. A **72** (2005) 013613.
- 17) J. Mur-Petit, A. Polls, and H.-J. Schulze: Phys. Lett. A **290** (2001) 317.
- 18) A. Bulgac, M.M. Forbes, and A. Schwenk: Phys. Rev. Lett. **97** (2006) 020402.
- 19) Y. Matsuda and H. Shimahara: J. Phys. Soc. Jpn. in press (cond-mat/0702481).
- 20) C.-C. Chien, Q. Chen, Y. He, and K. Levin: Phys. Rev. Lett. **97** (2006) 090402.
- 21) M. Iskin, and C.A.R. Sá de Melo: Phys. Rev. Lett. **97** (2006) 100404.
- 22) M. Mannarelli, G. Nardulli, and M. Ruggieri: Phys. Rev. A **74** (2006) 033606.
- 23) D.E. Sheehy and L. Radzihovsky: Phys. Rev. Lett. **96** (2006) 060401.
- 24) K. Yang, cond-mat/0508484.
- 25) H. Hu and X.-J. Liu: Phys. Rev. A **73** (2006) 051603(R).
- 26) C.-H. Pao, S.-T. Wu, and S.-K. Yip: Phys. Rev. B **73** (2006) 132506.
- 27) D.T. Son and M.A. Stephanov: Phys. Rev. A **74** (2006) 013614.
- 28) L. He, M. Jin, and P. Zhuang: Phys. Rev. B **73** (2006) 214527.
- 29) L. He, M. Jin, and P. Zhuang: Phys. Rev. B **74** (2006) 214516.
- 30) X. Huang, X. Hao, and P. Zhuang: cond-mat/0610610.
- 31) Q. Chen, Y. He, C.-C. Chien, and K. Levin: Phys. Rev. A **74** (2006) 063603.
- 32) Y. He, C.-C. Chien, Q. Chen, and K. Levin: Phys. Rev. A **75** (2007) 021602(R).
- 33) C.-C. Chien, Q. Chen, Y. He, and K. Levin: Phys. Rev. Lett. **97** (2006) 090402.
- 34) Z.-C. Gu, G. Warner, and F. Zhou: cond-mat/0603091.
- 35) P. Pieri and G.C. Strinati: Phys. Rev. Lett. **96** (2006) 150404.
- 36) P. Pieri and G.C. Strinati: cond-mat/0610675.
- 37) K. Machida and H. Nakanishi: Phys. Rev. B **30** (1984) 122.
- 38) N. Yoshida and S.-K. Yip: cond-mat/0703205.
- 39) W. Yi and L.-M. Duan: Phys. Rev. A **73** (2006) 031604(R).
- 40) W. Yi and L.-M. Duan: Phys. Rev. A **74** (2006) 013610.
- 41) M. Haquea and H.T.C. Stoof: Phys. Rev. A **74** (2006) 011602(R).
- 42) M. Haquea and H.T.C. Stoof: cond-mat/0701464.
- 43) T.N. De Silva and E.J. Mueller: Phys. Rev. A **73** (2006) 051602(R).
- 44) K.B. Gubbels, M.W.J. Romans, H.T.C. Stoof: Phys. Rev. Lett. **97** (2006) 210402.
- 45) J.-P. Martikainen: Phys. Rev. A **74** (2006) 013602.
- 46) C.-C. Chien, Q. Chen, Y. He, and K. Levin: Phys. Rev. A **74** (2006) 021602(R).
- 47) C.-C. Chien, Q. Chen, Y. He, and K. Levin: Phys. Rev. Lett. **98** (2007) 110404.
- 48) T. Mizushima, K. Machida, and M. Ichioka: Phys. Rev. Lett. **94** (2005) 060404.
- 49) K. Machida, T. Mizushima, and M. Ichioka: Phys. Rev. Lett. **97** (2006) 120407.
- 50) P. Castorina, M. Grasso, M. Oertel, M. Urban, and D. Zappalà: Phys. Rev. A **72** (2005) 025601.
- 51) X.-J. Liu, H. Hu, and P.D. Drummond: Phys. Rev. A **75** (2007) 023614.
- 52) J. Kinnunen, L.M. Jensen and P. Törmä: Phys. Rev. Lett. **96** (2006) 110403.
- 53) L. M. Jensen, J. Kinnunen, and P. Törmä: cond-mat/0604424.
- 54) P. G. de Gennes, *Superconductivity of Metals and Alloys* (Addison-Wesley, New York, 1989).
- 55) M. Randeria, J.-M. Duan, and L.-Y. Shieh: Phys. Rev. B **41**

- (1990) 327.
- 56) K. Huang: *Statistical Mechanics* (Wiley, New York, 1987).
 - 57) G. Bruun, Y. Castin, R. Dum, and K. Burnett: *Eur. Phys. J. D* **7** (1999) 433.
 - 58) A. Bulgac and Y. Yu: *Phys. Rev. Lett.* **88** (2002) 042504.
 - 59) M. Grasso and M. Urban: *Phys. Rev. A* **68**, 033610 (2003).
 - 60) G. A. Baker, Jr.: *Phys. Rev. C* **60** (1999) 054311.
 - 61) H. Heiselberg: *Phys. Rev. A* **63** (2001) 043606.
 - 62) A. J. Leggett: in *Modern Trends in the Theory of Condensed Matter*, edited by A. Pekalski and J. Przystawa (Springer, Berlin, 1980).
 - 63) R.B. Diener and T.-L. Ho: cond-mat/0405174.
 - 64) P. Pieri and G.C. Strinati: *Phys. Rev. Lett.* **91** (2003) 030401.
 - 65) G.B. Partridge, W. Li, R.I. Kamar, Y. an Liao, and R.G. Hulet: *Science* **311** (2005) 503.
 - 66) J.T. Stewart, J.P. Gaebler, C.A. Regal, and D.S. Jin: *Phys. Rev. Lett.* **97** (2006) 220406.
 - 67) The subroutine libraries are available from the ARPACK home page at <http://www.caam.rice.edu/software/ARPACK>.
 - 68) L. P. Gor'kov and T. K. Melik-Barkhudarov: *Sov. Phys. JETP* **13** (1961) 1018.
 - 69) A. Bulgac, J.E. Drut, and P. Magierski: *Phys. Rev. Lett.* **96** (2006) 090404.
 - 70) S. Kashiwaya and Y. Tanaka: *Rep. Prog. Phys.* **63** (2000) 1641.
 - 71) T. Mizushima, K. Machida, and M. Ichioka, *Phys. Rev. Lett.* **95**, 117003 (2005).
 - 72) A.I. Buzdin: *Rev. Mod. Phys.* **77** (2005) 935.
 - 73) Y. Ohashi and A. Griffin: *Phys. Rev. A* **72** (2005) 013601: (2005) 063606.
 - 74) M.A. Baranov: *Sov. Phys. JETP Lett.* **70** (1999) 396.
 - 75) C. Chin, M. Bartenstein, A. Altmeyer, S. Riedl, S. Jochim, J. Hecker Denschlag, and R. Grimm: *Science* **305** (2004) 1128.
 - 76) C.A. Regal and D. S. Jin: *Phys. Rev. Lett.* **90** (2003) 230404.
 - 77) S. Gupta, Z. Hadzibabic, M.W. Zwierlein, C.A. Stan, K. Dieckmann, C.H. Schunck, E.G.M. van Kempen, B.J. Verhaar, and W. Ketterle: *Science* **300** (2003) 1723.
 - 78) C.A. Regal, C. Ticknor, J.L. Bohn, and D.S. Jin: *Nature* **424** (2003) 47.
 - 79) G.M. Bruun, P. Törmä, M. Rodriguez, and P. Zoller: *Phys. Rev. A* **64** (2001) 033609.
 - 80) P. Törmä and P. Zoller: *Phys. Rev. Lett.* **85** (2000) 487.
 - 81) J. Kinnunen, M. Rodriguez, and P. Törmä: *Science* **305** (2004) 1131.
 - 82) N. Nygaard, G.M. Bruun, B.I. Schneider, C.W. Clark, and D.L. Feder: *Phys. Rev. A* **69** (2004) 053622.
 - 83) Y. He, Q. Chen, and K. Levin: *Phys. Rev. A* **72** (2005) 011602(R).
 - 84) J. Kinnunen and P. Törmä: *Phys. Rev. Lett.* **96** (2006) 070402.
 - 85) G.D. Mahan: *Many-Particle Physics* (Plenum Press, New York, 1990).
 - 86) P.M. Chaikin and T.C. Lubensky: *Principles of Condensed Matter Physics* (Cambridge Univ. Press, Cambridge, 1995).
 - 87) A.A. Abrikosov, L.P. Gor'kov, and I.E. Dzyaloshinski: *Methods of Quantum Field Theory in Statistical Physics* (Dover, New York, 1975).